A tree's view of the terrain: downscaling bioclimate variables to high resolution using a novel multi-level species distribution model

Matthew M. Kling[1†], Kathryn C. Baer[2], and David D. Ackerly[1,3]

[1]Dept. of Integrative Biology, University of California, Berkeley CA 94720[*]

[2]USDA Forest Service, Pacific Northwest Research Station Anchorage Forestry Sciences Laboratory, Anchorage, AK 99501

[3]Dept. of Environmental Science, Policy & Management, University of California, Berkeley CA 94720

[†]Email: mattkling@berkeley.edu

[*]Present address: Dept. of Biology and Gund Institute for the Environment, University of Vermont, Burlington VT 05405

Abstract

Fine-scale spatial climate variation fosters biodiversity and buffers it from climate change, but ecological studies are constrained by the limited accessibility of relevant fine-scale climate data. In this paper we introduce a novel form of species distribution model that uses species occurrences to predict high-resolution climate variation. This new category of "bioclimate" data, representing micro-scale climate as experienced by one or more species of interest, is a useful complement to microclimate data from existing approaches. The modeling method, called BISHOP for "Bioclimate Inference from Species' High-resolution Occurrence Patterns," uses data on species occurrences, coarse-scale climate, and fine-scale physiography (e.g. terrain, soil, vegetation) to triangulate fine-scale bioclimate patterns. It works by pairing a climate-downscaling function predicting a latent bioclimate variable, with a niche function predicting species occurrences from bioclimate. BISHOP infers how physiography affects bioclimate, estimates how these effects vary geographically, and produces high-resolution (10 m) maps of bioclimate over large regions. It also predicts species distributions.

After introducing this approach, we apply it in an empirical study focused on topography and trees. Using data on 216 North American tree species, we document the biogeographic patterns that enable BISHOP, we estimate how four terrain variables (northness, eastness, windward exposure, and elevational position) each influence three climate variables, and we use these results to produce downscaled maps of tree-specific bioclimate. Model validation demonstrates that inferred bioclimate outperforms macroclimate in predicting distributions of separate species not used during inference, confirming its ecological relevance. Our results show that nearby bioclimates can differ by 5°C in temperature and twofold in moisture, with equator-facing, east-facing, windward-facing, and locally-elevated sites exhibiting hotter, drier bioclimates on average. But these effects vary greatly across climate zones, revealing that topographically similar landscapes can differ strongly in their bioclimate variation. These results have important implications for micrometeorology, biodiversity, and climate resilience.

Introduction

Background: a climate data shortfall

Ecological patterns like species occurrences, population demographic rates, and vegetation gradients arise from organisms' experiences of environmental variation at extremely fine spatial scales, integrated over long temporal scales spanning the lifetimes of individuals and populations in a given location. Understanding the climate variation that drives these emergent phenomena is essential for basic ecology, and also for conservation, since climate heterogeneity helps to foster high biodiversity and buffer it from climate change (Dobrowski, 2011; Scherrer and Körner, 2011; McLaughlin et al., 2017; Suggitt et al., 2018; De Frenne et al., 2019). Yet we lack a category of spatial climate data that would be optimal for studying these biogeographic phenomena: data with high spatial resolution, low temporal resolution, and inherent ecological relevance to the species being studied.

Macroclimate data are the most readily-available and widely-used form of spatial climate data, and have a temporal scale ranging from years to decades that is well suited to studying time-integrated ecological patterns. But with a spatial resolution generally no finer than 1 km, these data capture only the climatic effects of coarse features like latitude, elevation, and continentality. They neglect microclimate patterns that arise from fine-scale physiographic features including terrain, vegetation, and soils that generate climate variation among nearby microsites (Geiger et al., 2009; Zellweger et al., 2020), an omission that has led to limitations and biases in global change research (Franklin et al., 2013; Potter et al., 2013; Nadeau et al., 2017).

Microclimate data do account for these fine-scale patterns and are becoming increasingly accessible (Bramer et al., 2018; Maclean et al., 2019; Lembrechts et al., 2020), but they have limitations. Mechanistic microclimate models that directly represent fine-scale meteorological physics have many advantages, but their accuracy depends on large volumes of high-resolution input data (e.g., leaf angle and leaf area index) that is often unavailable over large regions. Empirical models that correlate fine-scale variables like terrain and vegetation with measurements from *in situ* microclimate sensors offer a good solution (Bramer et al., 2018; John et al., 2024), but require that researchers either install their own sensors throughout a landscape of interest, or utilize global microclimate databases like SoilTemp (Lembrechts et al., 2020) that have geographic biases and may not be openly accessible.

Additionally, even with microclimate data in hand, barriers arise in incorporating them into many kinds of spatial ecological studies. Microclimate models typically produce high temporal frequency estimates of extremely specific meteorological variables (e.g., hourly time series of temperature 5 cm above the soil surface in a closed-canopy forest on particular dates (Maclean et al., 2019)), sometimes for numerous vertical strata across a site. Choosing among and summarizing these variables to match the temporal scale of ecological studies can be complex in both theory and practice. And while they may provide objective measures of certain aspects of the environment, a given variable may have limited relevance to the ecology of an individual species, especially considering the integrated impacts of environment on all aspects of the life history which determine whether a species is able to persist at a particular site.

Many of these issues can be addressed by using species occurrences themselves as climate indicators. Species occurrence data are widely available, are often highly localized (particularly for sessile organisms like plants), and integrate over ecological and physical uncertainties to capture the salient patterns of long-term climate variation as experienced by a species. There is a long history in ecology of using plants as climate indicators, including inferring climate from fossils ("paleoclimate proxies" (Lyell, 1837; Mauri et al., 2015)), from the performance of individuals transplanted into a site ("phytometers" (Clements and Goldsmith, 1924; Strobl et al., 2018)), and from the observed species composition of the naturally occurring plant community ("indicator species" (Ellenberg et al., 1992; Diekmann, 2003)). More recently, methods including latent-variable species distribution models (SDMs) (McInerny and Purves, 2011; Keil et al., 2013), climate indicator interpolation models (Karlsen et al., 2005; Scherrer and Körner, 2011), and microclimate heterogeneity estimators (Lenoir et al., 2013) have continued to expand the statistical tools available for using species occurrences to model fine-scale climate variation. But we are not aware of an existing approach that can use occurrences to predict and map high-resolution climate patterns, in native units like degrees Celsius, beyond the plots where species were recorded.

Novel method: refactoring an SDM to downscale climate variables

In this paper we introduce a new form of species distribution model that leverages species occurrence data, in combination with data on macroclimate and fine-scale physiography, to predict patterns of high-resolution climate as experienced by the focal species (fig. 1). We call this biologically inferred fine-scale climate variation "bioclimate", and we call the modeling method "bioclimate inference from species' high-resolution occurrence patterns" (BISHOP). The approach integrates components from a range of other methods, including indicator species models, latent-variable species distribution models, and empirical microclimate models.

A traditional SDM structure would either ignore micro-physiography or assume that it, along with macroclimate, directly predicts species occurrence probability. A BISHOP model instead assumes that macroclimate and micro-physiography shape an unmeasured bioclimate variable that then drives occurrence probability. The climate downscaling sub-model predicts a higher-resolution version of a macroclimate variable, creating its corresponding bioclimate variable by adding an offset (or Δ value) that is a function of fine-scale physiography (e.g. terrain, soils, vegetation). If one had field-based microclimate measurements, then the coefficients on these physiographic variables could be inferred as in a typical empirical microclimate model. Instead, these values are inferred from the occurrence patterns of one or more indicator species as is done in latent-variable SDMs (McInerny and Purves, 2011). The traditional SDM and BISHOP model both predict species occurrences from the same input variables, but in BISHOP's case predicting distributions is only an incidental side effect. BISHOP's primary, differentiating features are that it also predicts bioclimate, infers meaningful parameters quantifying how physiography shapes bioclimate, and infers a physiographically-controlled version of species climatic niches. It is thus useful as a tool for a range of applications separate from the traditional SDM.

This approach works by quantifying well-known relationships among macroclimate, fine-scale physiography, and species occurrences. Consider, for example, the general pattern (shown in the scatter plot in fig. 1) that across its geographic range, a plant species tends to be restricted to shadier pole-facing hillslopes in warm landscapes, to occupy a wide range of hillslopes in intermediate-temperature landscapes, and to be

restricted to sunnier equator-facing hillslopes in landscapes near its cold range limit (Boyko, 1947; Ackerly et al., 2020). These patterns presumably arise as a result of unmeasured fine-scale climate variation mediating the relationships between macroclimate, topography, and species occurrences. In this example, one could quantify the rate at which a species shifts onto increasingly pole-facing slopes as macroclimate warms (diagonal contours in fig. 1), which provides an estimate of how northness influences temperature from the perspective of the focal species. An effect size like this can be studied directly for its biological or meteorological interest, or used to generate downscaled bioclimate maps for other ecological applications.

Bioclimate inferred from species distributions could be a valuable complement to traditional microclimate estimates, helping fill the gap between existing macroclimate and microclimate data that limits research in biodiversity and conservation. These bioclimate variables are downscaled versions of the input macroclimate variables and carry the same units, but they are not directly comparable to traditional microclimate estimates, and the two should not be expected to precisely match. Instead, the bioclimate variables provide an inference or estimate of how the particular species of interest experiences fine-scale spatial climate variation integrated over long timeframes. Because not every species experiences microclimate in the same way, bioclimate variables will not necessarily be transferable among taxa.

While the above examples illustrate the simplest version of a BISHOP model, the model can be further extended. For example, the empirical analysis in this paper extends this model to a multivariate climate context, adds an additional model level representing how physiography-bioclimate parameters vary spatially as a function of other variables, and adds a hierarchical SDM module that allows multiple species to jointly inform the bioclimatic inferences (fig. S1). Although our analysis uses an unusually large multispecies data set, this is not a prerequisite for the BISHOP approach, which, like a traditional SDM, can be used on smaller datasets that are more readily available.

Empirical application: topography and trees

This modeling approach could be applied in a range of systems. Here, we use it to quantify how fine-scale terrain influences bioclimate from the perspective of tree species distributions across North America. Fine-scale presence-absence patterns of mature trees serve as an integrated indicator of all the microclimate conditions that influence a species' growth and survival, including the effects of underground, near-ground, and canopy-level microclimates on seedling, sapling, and adult trees.

We focus on three climate variables important to trees: summer daytime maximum temperature, winter nighttime minimum temperature, and annual precipitation (which for brevity we call "high temperature," "low temperature," and "moisture", respectively). Our analysis is based on 216 tree species across hundreds of thousands of plots surveyed for the USDA Forest Service Forest Inventory and Analysis Program (FIA) (Bechtold and Patterson, 2005) and Canada's National Forest Inventory (NFI) (Gillis et al., 2005). While the simultaneous use of many indicator species helps to refine bioclimate estimates and identify macroecological patterns, we also demonstrate use of the BISHOP approach with data for individual species.

Fine-scale terrain is a primary driver of microclimate variation in many regions (Geiger et al., 2009; Dobrowski, 2011). (Vegetation also plays a key microclimate role (De Frenne et al., 2019), and forest structure variables could easily be incorporated alongside terrain in this modeling framework, but since our study uses

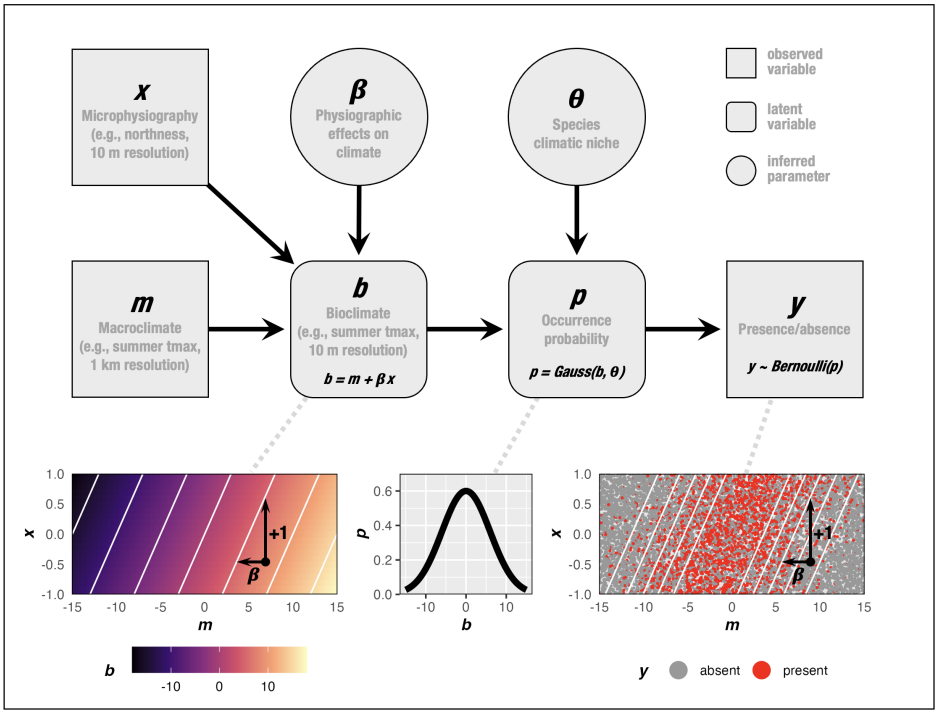

Figure 1: Structure of a BISHOP model, a form of SDM factored to infer and project high-resolution bioclimate in addition to species occurrence probability. The approach works by separating the typical SDM response function into two components: a bioclimate equation representing how fine-scale physiography (x, e.g. terrain, soil, or vegetation structure) modifies coarse-scale macroclimate (m, e.g. temperature or precipitation) to determine "bioclimate" (b, fine-scale climate as experienced by the species), and a niche equation representing how bioclimate predicts species occurrence probability (p). Arrows in the structural diagram indicate presumed causation. In the bottom row, the righthand plot shows an example relationship among the three input variables, with presences (red points) following a commonly-observed parallelogram shape in which species are increasingly restricted to north-facing slopes in macroclimatically warmer parts of their range (Ackerly et al., 2020). From this pattern, the model can jointly infer the species niche parameters (θ, describing the shape of a Gaussian bell curve illustrated at center) and the physiographic parameters (β, illustrated at left). This example uses a value of $\beta = -3$, which determines the angle of the isoclines shown in white on the lower plots. Note that while this figure illustrates a minimal version of the model, components can be added to accommodate multiple physiographic and climatic variables, multiple indicator species, and/or geographic variation in physiographic effects.

trees as indicator species we avoid vegetation predictors as they would introduce circularity.) We quantify how four terrain variables—northness, eastness, windward exposure, and elevational position relative to the surrounding landscape (fig. 2)—each influence the three climate variables mentioned above, for a total of 12 "topoclimate effects". These four micro-topographic axes influence a site's exposure to sun and wind as well as flows of air and water across the terrain, which in turn govern the temperature and moisture of its microclimate (fig. 2). The physical mechanisms connecting these terrain variables to microclimate are complex, involving interactions and feedbacks at multiple scales (Holland and Steyn, 1975; Dai et al., 1999; Geiger et al., 2009; Moeslund et al., 2013; Davis et al., 2019; Pastore et al., 2024). These direct effects also influence mediating variables like vegetation and soil that then themselves shape microclimate. (Boerner, 2006; Moeslund et al., 2013; Davis et al., 2019; De Frenne et al., 2019).

Importantly, these topoclimate effects are expected to vary geographically due to factors like sun angle, cloud cover, moisture availability, and wind regimes (Holland and Steyn, 1975; Dai et al., 1999; Geiger et al., 2009; Moeslund et al., 2013; Davis et al., 2019), and understanding this variation is a goal in ecology and micrometeorology. In our analysis we infer how each of the 12 topoclimate effects varies across climate zones as a function of two "modifier" variables: macroclimate temperature and precipitation. Temperature is an important predictor because phenomena like snow albedo feedbacks, latent heat flux, blackbody radiation rates, and sun angle differences (by correlation with latitude) vary across temperature gradients (Campbell and Norman, 2000; Geiger et al., 2009). Precipitation is expected to influence topoclimate effects because moisture alters the balance between sensible and latent heat fluxes and the balance among windward effects, and because associated cloud cover scatters incoming sunlight and reflects outgoing longwave radiation (Campbell and Norman, 2000; Geiger et al., 2009). Other important effect-modifying variables like latitude and cloud cover were not included directly because of their high correlations with temperature and precipitation, but they likely explain some of the inferred temperature and precipitation effects due to these correlations.

Our analysis has four empirical goals. First, we illustrate basic relationships between a landscape's macroclimate and the fine-scale topographic distributions of tree species within the landscape. Second, we use a BISHOP model to infer how the topographic variables affect each climate variable, and how these effects vary across climate zones. Third, we evaluate how these inferred bioclimates compare to macroclimate as predictors of tree species distributions. Lastly, we show how these results can be used to generate downscaled (10 m) maps of bioclimate as experienced by trees.

Methods

Species occurrences Our analysis is based on forest inventory data from FIA (Bechtold and Patterson, 2005) and NFI (Gillis et al., 2005). Seedling occurrences were not used since they may not reflect conditions suitable for long-term species persistence. From FIA we used the "tree" dataset; in addition to the main FIA dataset covering the continental US and coastal Alaska, we used FIA data from parts of interior Alaska. From NFI we used the ground plot "large trees" dataset. We excluded plots with stocking or harvesting, reconciled FIA-NFI taxonomy differences, and removed species with fewer than 100 occurrences. FIA plots each have four subplots, while NFI does not have subplots; we did all analyses at the FIA subplot and NFI plot level, and for simplicity refer to these as plots hereafter. For plots surveyed multiple times, we

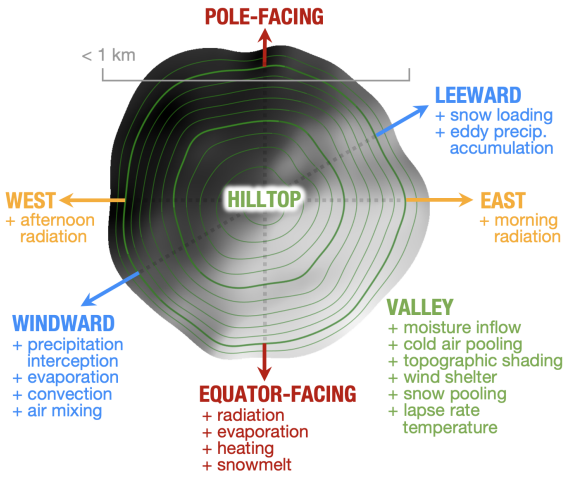

Figure 2: Processes through which fine-scale terrain shapes microclimate. Looking down on a hypothetical hill, arrows and contours illustrate the four topographic axes in our analysis, with micrometeorological rates listed at the end of the axes where they are expected to be higher. The north-south dimension is quantified as "northness," which measures how steeply a site faces the north. The east-west axis, "eastness," measures how steeply a site faces the east. "Windward exposure" indicates how steeply a site faces into the prevailing wind; the orientation of this axis varies but is pictured here as coming from the southwest since that is typical in our study area. Elevational position, the valley-hilltop axis sometimes called "topographic position index," is indicated by the contour lines and has low values at the bottom of all sides of this hill (the text placement is arbitrary). All four variables would have values of zero for a site in a uniformly level landscape.

considered a species present if it was recorded in any survey. We used confidential exact FIA and NFI plot locations.

Topoclimate variables We compiled several variables for each plot, including tree species occurrences, four *topographic variables* (northness, eastness, windward exposure, and elevational position (Theobald et al., 2015; USGS, 2019; Kling and Ackerly, 2020)), three primary *macroclimate variables* (total annual precipitation, maximum temperature of the warmest month, and minimum temperature of the coldest month (Karger et al., 2017)), and two *effect modifiers* (mean annual temperature and total annual precipitation). Whereas the "macroclimate variables" get modified by topography to become bioclimate variables and in turn shape species distributions, the "effect modifiers" are simply predictors that are hypothesized to influence the strength of those topoclimate effects; the modifiers we chose happen also to be climate variables, for the reasons described above. See Appendix 1.1–1.2 for details.

Data distillation Prior to modeling, we standardized all topographic and macroclimate variables. For each species, we generated a distinct occurrence dataset representing presences and absences across climatic and topographic gradients, and then summarized these continuous data into a set of discrete multivariate bins to reduce the dataset size for computational reasons. Data for all species were then combined into a single table. See Appendix 1.3 for details.

Species' topoclimate distributions To examine the relationships between a landscape's macroclimate and the topographic positions species occupy within the landscape, we grouped plots into bivariate macroclimate-by-topography bins and visualized the relative occurrence frequencies for each species in each bin. While these summaries are useful for illustrating topoclimate effects, a statistical model is needed to control for confounders such as spatial covariance or multivariate niche shapes.

Statistical bioclimate model We used the distilled data to fit a multilevel Bayesian model describing species occurrence probabilities as a function of macroclimate and topography. The model includes a climate downscaling component that models a latent bioclimate variable as a function of macroclimate and topography, and a niche component that models species occurrences as a function of bioclimate (figs. 1 & S1). By jointly inferring both sets of parameters, we can estimate the niche shapes and topoclimate effects that together best fit observed species occurrence patterns.

The model makes the following basic assumptions: 1) The difference between a site's macroclimate and its bioclimate is a function of topography. 2) Each macroclimate variable has a corresponding bioclimate variable, and these are equal in a flat site. 3) At a given site, each topographic variable has a linear modifying effect on each macroclimate variable. 4) These effects vary among locations as a spline function of the modifier variables. 5) The probability of a species occurring on a plot is a multivariate bell-shaped niche function of the plot's bioclimate. 6) Any additional variables omitted from the model are not correlated with the included variables in ways that would bias inference.

While none of these assumptions perfectly reflects the real world, they represent reasonable approximations that make the model tractable. For example, the second assumption that bioclimate and macroclimate are equal on a flat site is imperfect—microclimate is not simply fine-scale macroclimate—but adding an additional intercept term to account for the difference would make the model unidentifiable because the parameters for the intercept and the species niche optimum would be colinear.

We fit two versions of the model. In the "full" multi-species model that is the primary focus of our empirical results, data from all 216 species were jointly used to quantify bioclimate effects for North American trees and to infer how these effects vary as a function of modifier variables. In a second "minimal" version of the model that is simpler to implement in other studies, data from one species at a time was used to estimate average topography-microclimate effects across the species' range.

We evaluated model performance by examining MCMC diagnostics, by using simulated data to test parameter estimation, and by evaluating the model's ability to reproduce the "species topoclimate distributions" mentioned above. In addition, while BISHOP was conceived to study bioclimate rather than to predict species distributions, understanding its performance in predicting distributions is still informative. As a way to test the ecological relevance of BISHOP-inferred bioclimate variables, we compared the performance of bioclimate versus macroclimate as predictors of species occurrences. And as context for its utility as an SDM, we compared BISHOP to a standard SDM that was fit with the same macroclimate and topographic predictors but without the latent bioclimate component. Both these evaluations measured performance using cross-validation on withheld testing data. See Appendices 1.4–1.5 for details on model structure, fitting, and evaluation.

Climate downscaling We used the fitted multi-species model to generate downscaled tree-species bioclimate data for an example 6-by-13 km landscape in southern Idaho, USA (-112.65^{o}E, 42.56^{o}N). The inputs were the same macroclimate and wind data used to fit the model, and a 10 m elevation raster (USGS, 2019). We used bilinear interpolation to create smoothed macroclimate variables at 10 m resolution, and used elevation to calculate the four topographic variables at 10 m resolution. Using the fitted model parameters, we

then calculated bioclimate high temperature, low temperature, and moisture on the 10 m grid. This process is illustrated in figures 5 and S8.

This process can be easily replicated using an R package that accompanies this paper, available at `https://github.com/matthewkling/topoclimate.pred`, that lets users input elevation data for any landscape in our study area to generate bioclimate estimates for North American trees based on coefficients from the multi-species model. To yield consistent results, elevation data should have a resolution similar to our input data (10–100 m), and cover an area of multiple square kilometers. The model can provide reasonable estimates only within the continental US and Canada, so the tool does not allow extrapolation beyond this region.

All analysis was done in R (R Core Team, 2021) and Stan (Carpenter et al., 2017). Code, data, and results are available on GitHub at `https://github.com/matthewkling/topoclimate`.

Results

Species' topoclimate distributions

Forest inventory data show that for individual example species (fig. 3a-c) and the tree flora overall (fig. 3d), as a landscape becomes colder and/or moister, species occupy microsites that are more south-facing, more windward-facing, and more prominent. Individual species patterns differ from the average for reasons including differences in niche shapes, regional differences in topoclimate effects, and geographic differences in which terrain variables exhibit enough variation to have substantive microclimate effects.

Conceptually, topoclimate effects correspond to the horizontal shifts in these curves. For example, the relationship between northness and high temperature (top-center panel of fig. 3d) implies a difference of ∼2°C between steep north-facing and south-facing slopes, a value similar to published estimates from microclimate studies (Ashcroft et al., 2008; Bennie et al., 2008; Dobrowski et al., 2013). Note, however, that these marginal summaries cannot be interpreted directly as topoclimate effects due to confounding correlations.

Model evaluation

MCMC diagnostics indicated that the model mixed well, converged properly, and achieved good effective sample sizes (appendix 1.5). Testing on simulated data showed that the model accurately recovered known parameter values (fig. S12–S13). The model also reproduced the relationships shown in fig. 3, indicating it successfully captures the key patterns in the data set (Appendix 1.5; fig. S11).

Validation analyses (appendix 1.5) revealed that inferred fine-scale bioclimate variables outperform standard macroclimate variables in predicting independent species occurrences withheld from model fitting (fig. S14). This was true even across species boundaries, using bioclimate estimated from one set of species to predict distributions of separate species. Across all 16 variants of the validations, bioclimate outperformed macroclimate to a highly statistically significant degree (all Wilcoxon's $p \leq 1.1e^{-6}$; fig. S14). The fraction of species for which bioclimate outperformed macroclimate varied from 61.1% to 99.5% across metrics; bio-

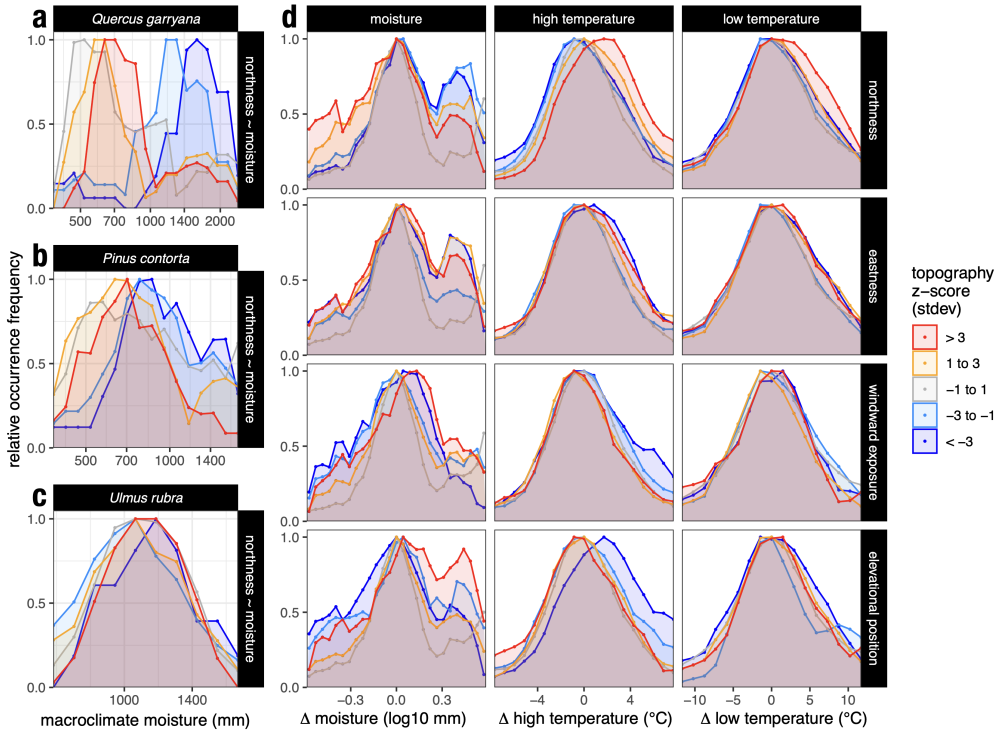

Figure 3: Species occurrence probability as a function of topography and macroclimate, summarized from forest inventory data without modeling. **(a-c)** Relationships between macroclimate moisture (x-axis) and northness (color) across the ranges of three example species; for a given combination of macroclimate and topographic values, y-values represent the relative proportion of forest inventory plots occupied by the species. These are specific cases of the general pattern shown in the upper-left panel of *d*. **(d)** Mean relationships across all 216 species in the analysis, for each combination of topographic variable (listed at right) and climate variable (listed at top); the macroclimate values on the x-axis represent the plot macroclimate minus the average macroclimate across plots occupied by a species. As an example to demonstrate interpretation, consider the bottom-center panel of *d*, which shows relationships between macroclimate summer high temperature (x-axis) and plot elevational position (color): the horizontal offset between the dark red curve (highly prominent sites) and dark blue curve (highly depressed sites) indicates that the difference between these topographic positions corresponds to roughly 3°C on average, while the vertical differences indicate that for example in a landscape 6°C hotter than its average, the typical species is roughly three times more likely to occur in a highly depressed plot as a highly prominent plot. Topographic variables are standardized for comparability.

climate model performance was generally higher for within-sample tests than out-of-sample tests, and for the minimal single-species model than the full multi-species model (fig. S14).

We also found that single-species BISHOP models on average outperformed a standard SDM (fit with the same macroclimate and topographic predictors but lacking the bioclimate interaction term) in predicting species occurrences during cross-validation. Across species, the difference was significant when measuring performance with predictive AUC but not with log likelihood (Wilcoxon's $p = 0.003$ and 0.396, respectively; fig. S15).

Topoclimate effects

For most of the 12 topoclimate relationships, we found strong support for ecologically meaningful effect sizes, as well as major variation in effects across climate zones (fig. 4).

Northness Northness strongly influenced tree bioclimate, with north-facing microsites almost universally cooler and wetter than their south-facing counterparts (fig. 4). A unit increase in northness (equivalent to north- versus south-facing 30° slopes; fig. S7) was associated with up to 43% higher moisture, 3.2°C lower high temperature, and 2.5°C lower low temperature. Northness had its greatest effect on bioclimatic moisture and high temperature in cool-dry regions, and its weakest effect on low temperature in these same regions.

Eastness Eastness had generally smaller effects than northness (fig. 4). On average, east-facing microsites were ecologically drier and warmer, with a unit increase in eastness showing up to 11% lower moisture and up to 2.3°C higher high temperature, and with both effects once again strongest in cool-dry macroclimates. Eastness impacts on low temperatures were smaller and more mixed. Combining eastness and northness, we found that in most contexts the three bioclimate variables are maximized in distinct compass directions (fig. S4).

Wind Windward exposure also showed strong tree bioclimate signatures (fig. 4). Windward slopes were ecologically drier and warmer than leeward slopes on average, with a unit increase in windward exposure associated with up to 15% lower moisture, up to 0.7°C higher high temperature, and up to 1.9°C higher low temperature. But there was major regional variation, with wind's strongest warming effect on high temperature in cold-dry regions, its strongest warming effect on low temperature in warm-wet regions, and its strongest drying effect in cold-wet regions. In warm-wet regions, windward exposure switched effect directions and had a strong positive impact on moisture signatures.

Importantly, the observed effects of windward exposure could be confounded with the effects of northness and eastness, since prevailing wind patterns mean that windward exposure is often highest on the same southwest slopes that experience maximum afternoon insolation. To explore this issue, we fit a second model omitting windward exposure; it had very similar but slightly larger northness and eastness parameters (fig. S5), which we take to mean that wind-sun correlations are a real but relatively minor driver of our results. This correlation should be kept in mind when interpreting northness and eastness effects as well; it is impossible to fully separate sun- and wind-based phenomena here, although data from other regions could help disentangle

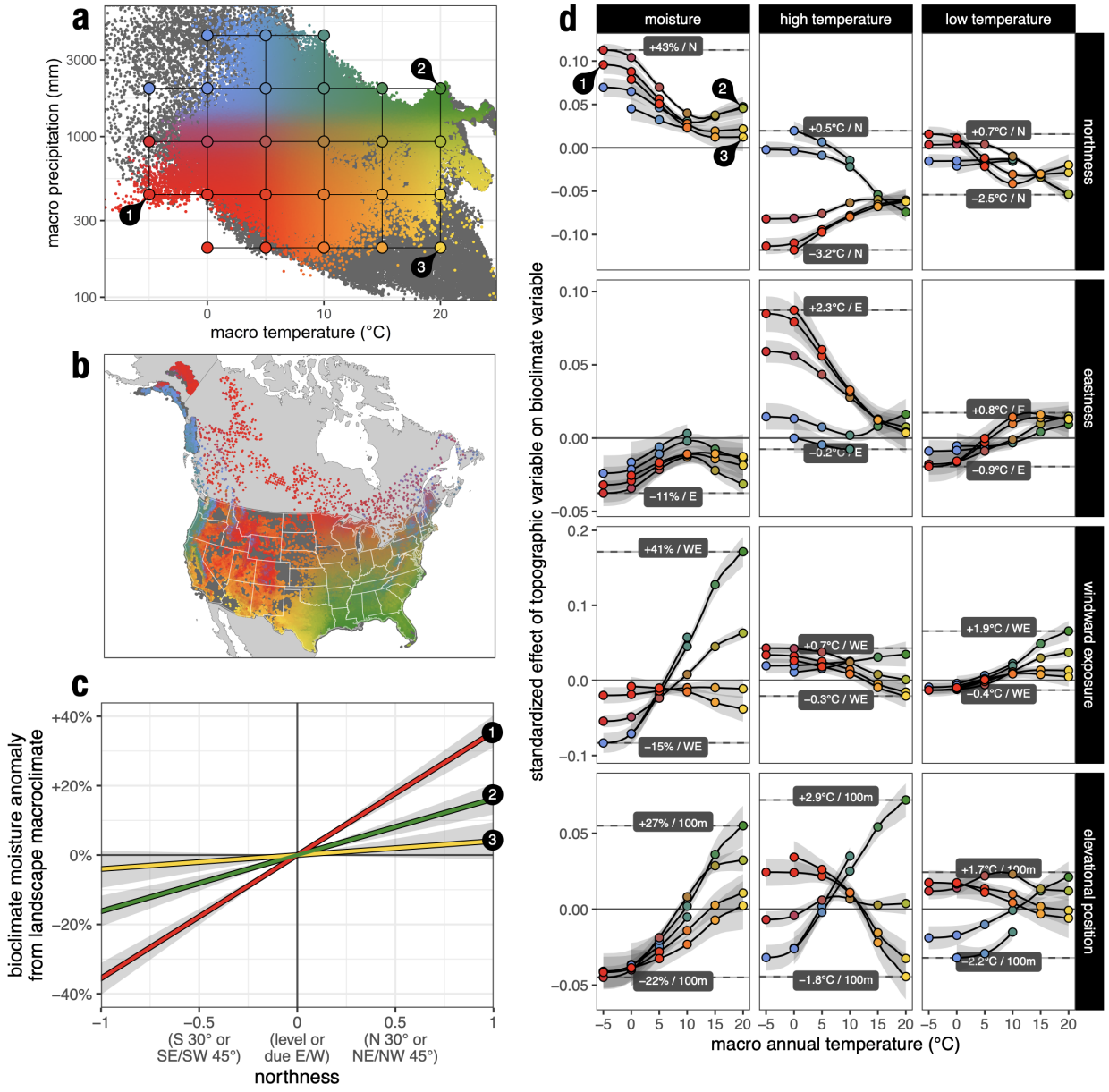

Figure 4: Effects of fine-scale topography on bioclimate, inferred from tree species distributions. **(a-b)** Macroclimate and location of survey plots, colored by macro-scale temperature and precipitation ("effect modifier" variables in our analysis); colored points are forest plots and dark gray are non-forest plots. The colors correspond to the x- and y-axes of panel *a*, which are then used to illustrate results in the other panels. The reference grid of larger points in panel *a* corresponds to the points in *d*. **(c)** Examples of inferred northness-moisture relationships under three different macroclimates (annotated ①–③ in panels *a*, *c*, and *d*); x-values represent the northness of a microsite, and y-values represent its bioclimate moisture anomaly (or Δ) relative to macroclimate precipitation, which is assumed to be zero for level sites; the *slopes* of these lines are the "topoclimate effects," which vary across climate zones. **(d)** Fitted values for topoclimate effects; each y-axis value is the slope of the linear relationship (illustrated in *c*) between the topographic variable listed at top and the microclimate variable listed at right; these effects vary as a function of macroclimate, as indicated by x-axis values and colors. The y-axis shows standardized effects for comparability across variables, while variable-specific units are annotated within each panel (e.g., the reference line in the upper-right panel marked "-2.5°C / N" indicates that low temperature decreases by 2.5°C when northness increases by 1). Lines in panels *c*-*d* show posterior medians, while shaded ribbons show 95% posterior credibility intervals. As an **example to demonstrate interpretation**, consider the effect of northness on moisture, depicted in the upper left panel of *d* and further illustrated in *c*: the inferred effect (slopes in *c*, y-values in *d*) is positive across all climate zones, but greatest in cool-dry macroclimates (red; ①), where a unit increase in northness (which equates to the difference between south- and north-facing 30° slopes as seen on the x-axis of *c*) corresponds to a +35% increase in moisture.

them. Fortunately, there is virtually no correlation among northness, eastness, and elevational position, so this issue is limited to windward exposure.

Elevational position Elevational position within a landscape was also associated with highly context-dependent effects on tree bioclimate (fig. 4). On average, prominences had drier, warmer signatures than their surroundings, but this varied substantially across climate zones. A site 100 m higher than its neighborhood had ecological moisture levels ranging from 27% wetter to 22% drier, maximum temperatures ranging from 2°C cooler to 3°C hotter, and minimum temperatures ranging from 2.3°C colder to 1.7°C warmer.

Species niches The final set of model parameters is a three-dimensional bioclimate niche for each species, and we found substantial variation in the position, size and shape of these niches (fig. S6). We do not elaborate on these results here, as they are not the focus of this paper.

Single-species models In addition to the full multi-species model, we fit a separate minimal model for each species. There was substantial variation in topoclimate effects across species, but general agreement between the median effect and the results of the full model (fig. S2). Each of three example species exhibited highly credible effects (95% posterior CI's not overlapping zero) for a subset of the 12 topoclimate coefficients (fig. S2).

Comparing each species' topoclimate coefficients to the average temperature and precipitation across its range, we find clear trends across macroclimate gradients for many of the 12 effects (fig. S3). In cases where these relationships are significant (slopes whose 95% CI's do not contain zero, fig. S3), they tend to match the macroclimate trends captured in the full multi-species model (fig. 4d).

Climate downscaling

We demonstrated the downscaling process by producing 10 m resolution bioclimate variables for an example landscape (figs. 5 and S8). They show much higher levels of fine-scale variation than does a simple interpolation of macroclimate, and 83% of bioclimate values are outside the convex hull of macroclimate values over this landscape (fig. 5d).

Discussion

This work helps to fill a gap in traditional high-resolution climate modeling approaches, demonstrating that abundantly available species distribution data can be used to infer biologically salient climate patterns at microclimate scales.

Our empirical results illustrate general biogeographic patterns in tree species topographic distributions, quantify strong and regionally variable effects of topography on fine-scale bioclimate as experienced by trees, and enable the creation of high-resolution maps of bioclimate for tree species. Our model validations show that these bioclimate variables better predict out-of-sample occurrences not just for the species used to fit a given model but also for entirely separate tree species (fig. S14), indicating they capture aspects of microclimate variation that are broadly relevant across tree species.

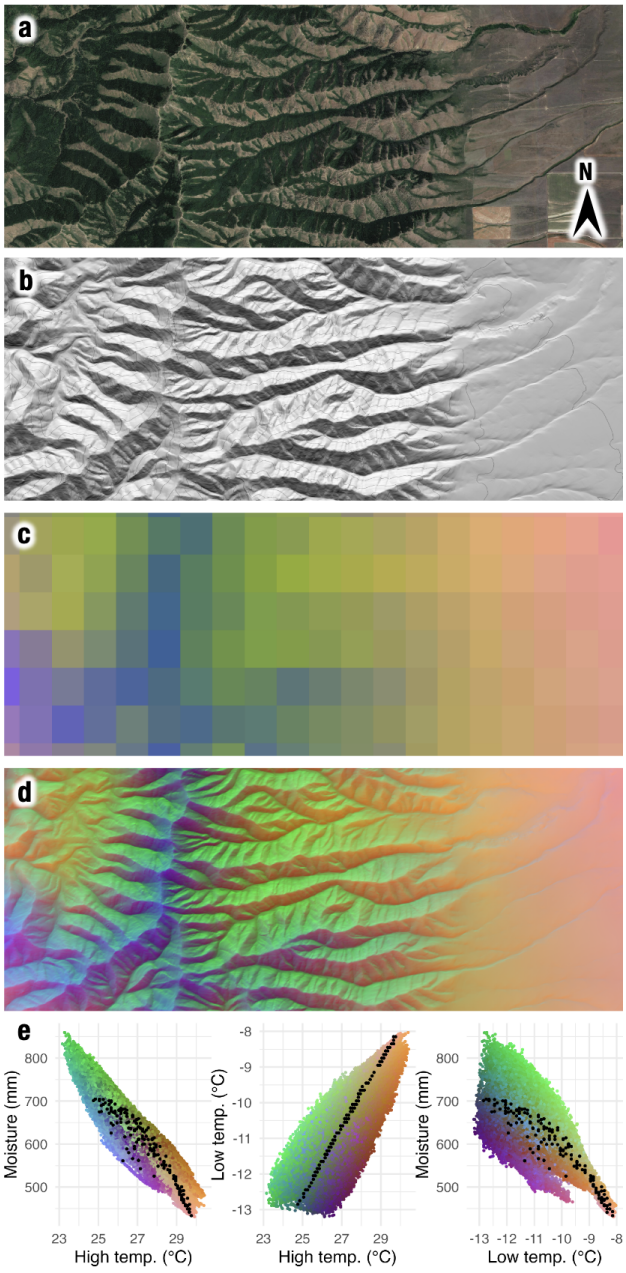

Figure 5: Example of a downscaled 10 m resolution bioclimate map for a rugged 6-by-13 km landscape in southern Idaho, USA, created using the BISHOP model in our analysis. Values represent long-term climate means from 1979–2009. **(a)** Satellite photo of the landscape, from Google Earth, showing the distribution of forest restricted to north-facing slopes and drainages, where microclimates are presumably more suitable; subtler east-west difference are also visible. **(b)** Shaded relief map of topography across the landscape, based on a digital elevation model with 10 m resolution. **(c)** Macroclimate data at 1 km resolution, with colors representing unique combinations of high temperature, low temperature, and moisture (i.e. precipitation) as shown in *e*. **(d)** Model estimates of bioclimate experienced by trees, made using *b*, *c*, and posterior modes from the fitted model parameters from our analysis; colors represent bioclimate as shown in *e*. **(e)** Bivariate scatter plots of climate values across the landscape, with colored points representing bioclimate values from panel *d* and black points representing macroclimate values from panel *c*.

Our results are directly relevant to the North American tree species we used as indicators. Although our species-level cross-validation analyses indicate that these bioclimate inferences often transfer well to tree species not used in model fitting, it should not be assumed that they would extrapolate well to other regions or taxa. For applications in other study systems, it would be necessary to empirically test the utility of these tree-derived variables, or to fit a new BISHOP model to derive bioclimate variables tailored to that system.

While bioclimatic inferences built upon tree distributions may not be applicable to other study systems, the BISHOP methodology we introduce could be applied in a range of other domains including for different taxa, physiographic variables, indicator data types, and temporal scales. For example, a study focused on understory plants might use forest structure and soil as physiographic predictors instead of terrain, a study using animal movement data as a bioclimate indicator might downscale sub-hourly weather instead of multidecadal climatologies, or a grassland phenology study might relate terrain to remote-sensed spring green-up dates over an individual season. Even more generally, the notion of a regression model predicting a latent environmental variable that in turn predicts an ecological outcome could have applications beyond inferring fine-scale climate patterns.

Species niches and distributions While BISHOP was designed principally for inferring bioclimate patterns, not for the traditional SDM goals of inferring climatic niches and predicting species distributions, it is also applicable for those purposes. The niches we inferred for each tree species (fig. S6) are explicitly a function of micro-scale bioclimate rather than macroclimate, and earlier studies have found that similarly derived niche estimates better reflect species' true relationships with climate (McInerny and Purves, 2011; Keil et al., 2013). Our results showed that realized macroclimate niche breadths are narrower when controlling for topography than when averaging across it (fig. 3), suggesting the latter approach would overestimate true niche breadth.

Many prior SDM studies have used terrain variables alongside macroclimate to improve predictive performance. BISHOP demonstrated this same improvement during cross-validation on withheld testing data, performing substantially better on average than SDMs with only macroclimate predictors, and slightly better than SDMs with the same macroclimate and terrain predictors but no latent bioclimate variables. This latter result is not decisive enough to recommend BISHOP over standard methods for studies in which the goal is predicting species occurrences and bioclimate is not of interest for its own sake, but it does suggest that the approach fits the occurrence data relatively well and makes useful SDM predictions.

We note that caution should be taken to avoid circularity that could arise if a BISHOP model were used to predict bioclimate variables, which were then used as predictors in a subsequent SDM. Like suitability predictions, these bioclimate predictions are an SDM output that is not independent of the occurrence data points used in fitting the BISHOP model, which could result in misleading validation metrics if the same occurrence data were used in the subsequent model.

Climate downscaling Using the fitted model and accompanying R package to downscale macroclimate data, we identified substantial tree bioclimate variation within the example landscape (fig. 5d). Visually, the downscaled bioclimate data better matches the striking vegetation patterns in this landscape than does the macroclimate data, indicating its likely utility in spatial modeling. In spite of substantial macroclimate

variation within this landscape, the large majority of bioclimate values fall outside the observed range of macroclimate values (fig. 5e), indicating major potential for macroclimate to overlook suitable habitat and to underestimate species persistence under climate change.

Fine-sale bioclimate variables like these could be used in a range of applications requiring data on spatial climate variation, including studies on biogeography, demography, and physiology. As noted above, use of BISHOP-derived bioclimate variables as predictors in subsequent SDMs should be done only with caution, in order to avoid circularity.

While there is no expectation that bioclimate variables like these should precisely match traditional microclimate variables, it would still be informative for future studies to compare the two approaches across different landscapes. Investigating the situations in which bioclimate and microclimate do and to not align could help to uncover important patterns in species climate sensitivity, to identify the microclimate variables most relevant to different taxa, and to identify when bioclimate may be useful as a predictor of microclimate.

Topoclimate effects Beyond their use for downscaling, the inferred topoclimate parameters themselves reveal how different physiographic features shape bioclimate and how these effects vary geographically, topics that have become a focus for their importance to biodiversity and climate vulnerability (Dobrowski, 2011; Moeslund et al., 2013).

Our analysis found that north-facing slopes were almost universally ecologically cooler and wetter than south-facing slopes (fig. 4), consistent with expectations based on increased insolation on equator-facing slopes. The greatest effects of northness on moisture and high temperature were seen in cool-dry landscapes, perhaps due to factors like greater topographic insolation contrast at higher latitudes (Holland and Steyn, 1975) and greater scattering of direct solar radiation in cloudier regions (Dai et al., 1999). In the coolest-wettest climates, the effect of northness on bioclimatic high temperature disappeared entirely, perhaps because persistent moisture in these landscapes leads insolation to drive melting and evaporation rather than raise temperatures (Dai et al., 1999; Dobrowski, 2011). The effect of northness on low temperature was weakest in the same cold-dry regions where its high temperature effect was strongest, perhaps due to weaker physical mechanisms (e.g. to snow albedo mitigating warming) or to lower importance of winter minimum temperatures for tree physiology (e.g. because they are dormant and/or cold-hardy) (Nobel and Linton, 1997).

Eastness had generally smaller effects than northness, with east-facing slopes warmer and drier than west-facing slopes on average (fig. 4). Given that micrometeorological studies commonly find the highest temperatures on southwest slopes, which has led to wide use of topographic heat load variables oriented on a southwest-northeast axis (McCune and Keon, 2002), our finding that southeast slopes had the hottest-driest signatures may seem surprising. Yet our result is consistent with prior findings that vegetation cover is lowest on southeast-facing slopes in this region (Smith and Bookhagen, 2021) and that trees often have slower growth and regeneration on southeast-facing slopes (Kelsey et al., 2018; Redmond and Kelsey, 2018). Two factors could drive these patterns: east slopes can genuinely be hotter where cloud cover and precipitation occur predominantly in the afternoon (Geiger et al., 2009), and trees can simply be more sensitive to morning- than afternoon climate because they are more physiologically active in the morning (Johnson et al.,

2009; Kelsey et al., 2018). Whatever the cause, these findings call into question conventional assumptions about southwest aspects in ecology.

Our results also highlight that the three bioclimate variables each have distinct relationships with aspect (fig. S4), meaning that no individual axis is adequate to describe the multidimensional bioclimate variation found around the circumference of a given hill. This finding is consistent with studies showing that different measures of tree physiology, which are presumably sensitive to different climate variables, reach their maxima on distinct aspects (Stage, 1976).

Both windward slopes and locally-elevated sites had warmer and drier bioclimates on average, but there was major regional variation in both effects. These results likely reflect the many, often countervailing, mechanisms by which wind and elevational position influence microclimate (fig. 2). While wind likely drives higher evaporation rates on windward slopes in most situations, it can deliver more precipitation to either windward or leeward hillslopes, and can cause either convective warming or cooling. Compared to depressions, prominences can receive more precipitation but can lose it more quickly due to snow drifting and (sub)surface flow; they are generally windier, which could lead to positive or negative impacts on both temperature and moisture for the reasons discussed above; and they can be cooler due to the lapse rate or warmer due to cold air pooling and reduced shading. Our results demonstrate that the balance among these countervailing phenomena, and/or trees' relative sensitivity to these phenomena, varies across climate zones.

Implications for biodiversity and climate change Topographically heterogeneous areas are often prioritized in conservation planning because topography generates microclimate heterogeneity (Lawler et al., 2015), which in turn fosters biodiversity by increasing available niche space and reduces local extinction under climate change by generating microrefugia and reducing climate velocities (Loarie et al., 2009; Dobrowski, 2011; McLaughlin et al., 2017; Suggitt et al., 2018). Our results help to refine estimates of the relationships between topography and these features of biodiversity maintenance.

We found that each bioclimate variable has distinct relationships with the four topographic variables (fig. 4). This means that topography generates multidimensional bioclimate variation within a landscape, which is important because species adapting to climate change face challenges from the need to simultaneously track multiple climate variables changing in different ways (Dobrowski et al., 2013; Hamann et al., 2015; Ordonez et al., 2016).

We also found major variation in topoclimate effects across climate zones (fig. 4). This implies that identical terrain in different spatial (and perhaps temporal) contexts generates different amounts of biotically relevant microclimate variation. Spatially, this means for example that landscapes in cold-dry regions, which had substantially larger topoclimate effects than cold-wet regions, may see lower tree bioclimatic velocities and more microrefugia as climate changes, per unit of topographic heterogeneity. Temporally, if we apply space-for-time substitution to, for example, the finding that cooler landscapes have steeper northness-moisture relationships, it could imply that the expected degree of bioclimatic moisture heterogeneity within individual landscapes may decline under global warming, reducing their capacity to support tree biodiversity. Further research should investigate how these trends in topoclimate effects shape observed biodiversity dynamics over space and time.

References

Ackerly, David D, Matthew M Kling, Matthew L Clark, Prahlad Papper, Meagan F Oldfather, Alan L Flint, and Lorraine E Flint (2020). "Topoclimates, refugia, and biotic responses to climate change". In: *Frontiers in Ecology and the Environment* 18.5, pp. 288–297.

Ashcroft, Michael B, Laurie A Chisholm, and Kristine O French (2008). "The effect of exposure on landscape scale soil surface temperatures and species distribution models". In: *Landscape Ecology* 23.2, pp. 211–225.

Bechtold, William A and Paul L Patterson (2005). *The enhanced Forest Inventory and Analysis program—national sampling design and estimation procedures*. 80. USDA Forest Service, Southern Research Station.

Bennie, Jonathan J, Brian Huntley, Andrew Wiltshire, Mark O Hill, and Robert Baxter (2008). "Slope, aspect and climate: spatially explicit and implicit models of topographic microclimate in chalk grassland". In: *Ecological Modelling* 216.1, pp. 47–59.

Boerner, RE J (2006). "Unraveling the Gordian Knot: interactions among vegetation, topography, and soil properties in the central and southern Appalachians". In: *The Journal of the Torrey Botanical Society* 133.2, pp. 321–361.

Boyko, Hugo (1947). "On the role of plants as quantitative climate indicators and the geo-ecological law of distribution". In: *The Journal of Ecology* 35, pp. 138–157.

Bramer, Isobel, Barbara J Anderson, Jonathan J Bennie, Andrew J Bladon, Pieter De Frenne, Deborah Hemming, Ross A Hill, Michael R Kearney, Christian Körner, Amanda H Korstjens, et al. (2018). "Advances in monitoring and modelling climate at ecologically relevant scales". In: *Advances in Ecological Research*. Vol. 58. Elsevier, pp. 101–161.

Campbell, Gaylon S and John M Norman (2000). *An introduction to environmental biophysics*. Springer Science & Business Media.

Carpenter, Bob, Andrew Gelman, Matthew D Hoffman, Daniel Lee, Ben Goodrich, Michael Betancourt, Marcus Brubaker, Jiqiang Guo, Peter Li, and Allen Riddell (2017). "Stan: A probabilistic programming language". In: *Journal of Statistical Software* 76.1.

Clements, Frederic Edward and Glenn Warren Goldsmith (1924). *The phytometer method in ecology: the plant and community as instruments*. 356. Carnegie Institution of Washington.

Dai, Aiguo, Kevin E Trenberth, and Thomas R Karl (1999). "Effects of clouds, soil moisture, precipitation, and water vapor on diurnal temperature range". In: *Journal of Climate* 12.8, pp. 2451–2473.

Davis, Kimberley T, Solomon Z Dobrowski, Zachary A Holden, Philip E Higuera, and John T Abatzoglou (2019). "Microclimatic buffering in forests of the future: the role of local water balance". In: *Ecography* 42.1, pp. 1–11.

De Frenne, Pieter, Florian Zellweger, Francisco Rodrıguez-Sánchez, Brett R Scheffers, Kristoffer Hylander, Miska Luoto, Mark Vellend, Kris Verheyen, and Jonathan Lenoir (2019). "Global buffering of temperatures under forest canopies". In: *Nature Ecology & Evolution* 3.5, pp. 744–749.

Diekmann, Martin (2003). "Species indicator values as an important tool in applied plant ecology—a review". In: *Basic and Applied Ecology* 4.6, pp. 493–506.

Dobrowski, Solomon Z (2011). "A climatic basis for microrefugia: the influence of terrain on climate". In: *Global Change Biology* 17.2, pp. 1022–1035.

Dobrowski, Solomon Z, John Abatzoglou, Alan K Swanson, Jonathan A Greenberg, Alison R Mynsberge, Zachary A Holden, and Michael K Schwartz (2013). "The climate velocity of the contiguous United States during the 20th century". In: *Global Change Biology* 19.1, pp. 241–251.

Ellenberg, HEINZ, HEINRICH E Weber, RUBRECHT Düll, VOLKMAR Wirth, WILLY Werner, and DIRK Paulißen (1992). "Zeigerwerte von pflanzen in mitteleuropa. Scripta Geobotanica 18". In: *Göttingen, Goltze*.

Franklin, Janet, Frank W Davis, Makihiko Ikegami, Alexandra D Syphard, Lorraine E Flint, Alan L Flint, and Lee Hannah (2013). "Modeling plant species distributions under future climates: how fine scale do climate projections need to be?" In: *Global Change Biology* 19.2, pp. 473–483.

Geiger, Rudolf, Robert H Aron, and Paul Todhunter (2009). *The Climate Near the Ground*. Rowman & Littlefield.

Gillis, Mark D, AY Omule, and T Brierley (2005). "Monitoring Canada's forests: the National Forest Inventory". In: *The Forestry Chronicle* 81.2, pp. 214–221.

Hamann, Andreas, David R Roberts, Quinn E Barber, Carlos Carroll, and Scott E Nielsen (2015). "Velocity of climate change algorithms for guiding conservation and management". In: *Global Change Biology* 21.2, pp. 997–1004.

Holland, PG and DG Steyn (1975). "Vegetational responses to latitudinal variations in slope angle and aspect". In: *Journal of Biogeography* 2, pp. 179–183.

John, Aji, Julian D Olden, Meagan F Oldfather, Matthew M Kling, and David D Ackerly (2024). "Topography influences diurnal and seasonal microclimate fluctuations in hilly terrain environments of coastal California". In: *PLOS One* 19.3, e0300378.

Johnson, Daniel M, David R Woodruff, Katherien A McCulloh, and Frederick C Meinzer (2009). "Leaf hydraulic conductance, measured in situ, declines and recovers daily: leaf hydraulics, water potential and stomatal conductance in four temperate and three tropical tree species". In: *Tree Physiology* 29.7, pp. 879–887.

Karger, Dirk Nikolaus, Olaf Conrad, Jürgen Böhner, Tobias Kawohl, Holger Kreft, Rodrigo Wilber Soria-Auza, Niklaus E Zimmermann, H Peter Linder, and Michael Kessler (2017). "Climatologies at high resolution for the earth's land surface areas". In: *Scientific Data* 4.1, pp. 1–20.

Karlsen, Stein Rune, Arve Elvebakk, and Bernt Johansen (2005). "A vegetation-based method to map climatic variation in the arctic–boreal transition area of Finnmark, north-easternmost Norway". In: *Journal of Biogeography* 32.7, pp. 1161–1186.

Keil, Petr, Jonathan Belmaker, Adam M Wilson, Philip Unitt, and Walter Jetz (2013). "Downscaling of species distribution models: a hierarchical approach". In: *Methods in Ecology and Evolution* 4.1, pp. 82–94.

Kelsey, Katharine C, Miranda D Redmond, Nichole N Barger, and Jason C Neff (2018). "Species, climate and landscape physiography drive variable growth trends in subalpine forests". In: *Ecosystems* 21.1, pp. 125–140.

Kling, Matthew M and David D Ackerly (2020). "Global wind patterns and the vulnerability of wind-dispersed species to climate change". In: *Nature Climate Change* 10.9, pp. 868–875.

Lawler, Joshua J, David D Ackerly, Christine M Albano, Mark G Anderson, Solomon Z Dobrowski, Jacquelyn L Gill, Nicole E Heller, Robert L Pressey, Eric W Sanderson, and Stuart B Weiss (2015). "The theory behind, and the challenges of, conserving nature's stage in a time of rapid change". In: *Conservation Biology* 29.3, pp. 618–629.

Lembrechts, Jonas J, Juha Aalto, Michael B Ashcroft, Pieter De Frenne, Martin Kopeckỳ, Jonathan Lenoir, Miska Luoto, Ilya MD Maclean, Olivier Roupsard, Eduardo Fuentes-Lillo, et al. (2020). "SoilTemp: A global database of near-surface temperature". In: *Global Change Biology* 26.11, pp. 6616–6629.

Lenoir, Jonathan, Bente Jessen Graae, Per Arild Aarrestad, Inger Greve Alsos, W Scott Armbruster, Gunnar Austrheim, Claes Bergendorff, H John B Birks, Kari Anne Bråthen, Jörg Brunet, et al. (2013). "Local temperatures inferred from plant communities suggest strong spatial buffering of climate warming across N orthern E urope". In: *Global Change Biology* 19.5, pp. 1470–1481.

Loarie, Scott R, Philip B Duffy, Healy Hamilton, Gregory P Asner, Christopher B Field, and David D Ackerly (2009). "The velocity of climate change". In: *Nature* 462.7276, pp. 1052–1055.

Lyell, Charles (1837). *Principles of geology: Being an inquiry how far the former changes of the Earth's surface are referable to causes now in operation*. Vol. 1. J. Kay, jun. & brother.

Maclean, Ilya MD, Jonathan R Mosedale, and Jonathan J Bennie (2019). "Microclima: An R package for modelling meso-and microclimate". In: *Methods in Ecology and Evolution* 10.2, pp. 280–290.

Mauri, A, BAS Davis, PM Collins, and Jed O Kaplan (2015). "The climate of Europe during the Holocene: a gridded pollen-based reconstruction and its multi-proxy evaluation". In: *Quaternary Science Reviews* 112, pp. 109–127.

McCune, Bruce and Dylan Keon (2002). "Equations for potential annual direct incident radiation and heat load". In: *Journal of Vegetation Science* 13.4, pp. 603–606.

McInerny, Greg J and Drew W Purves (2011). "Fine-scale environmental variation in species distribution modelling: regression dilution, latent variables and neighbourly advice". In: *Methods in Ecology and Evolution* 2.3, pp. 248–257.

McLaughlin, Blair C, David D Ackerly, P Zion Klos, Jennifer Natali, Todd E Dawson, and Sally E Thompson (2017). "Hydrologic refugia, plants, and climate change". In: *Global Change Biology* 23.8, pp. 2941–2961.

Moeslund, Jesper Erenskjold, Lars Arge, Peder Klith Bøcher, Tommy Dalgaard, and Jens-Christian Svenning (2013). "Topography as a driver of local terrestrial vascular plant diversity patterns". In: *Nordic Journal of Botany* 31.2, pp. 129–144.

Nadeau, Christopher P, Mark C Urban, and Jon R Bridle (2017). "Coarse climate change projections for species living in a fine-scaled world". In: *Global Change Biology* 23.1, pp. 12–24.

Nobel, Park S and Matthew J Linton (1997). "Frequencies, microclimate and root properties for three codominant perennials in the northwestern Sonoran Desert on north- vs. south-facing slopes". In: *Annals of Botany* 80.6, pp. 731–739.

Ordonez, Alejandro, John W Williams, and Jens-Christian Svenning (2016). "Mapping climatic mechanisms likely to favour the emergence of novel communities". In: *Nature Climate Change* 6.12, pp. 1104–1109.

Pastore, Melissa A, Aimée T Classen, Anthony W D'Amato, Marie E English, Karin Rand, Jane R Foster, and E Carol Adair (2024). "Frequent and strong cold-air pooling drives temperate forest composition". In: *Ecology and Evolution* 14.4, e11126.

Potter, Kristen A, H Arthur Woods, and Sylvain Pincebourde (2013). "Microclimatic challenges in global change biology". In: *Global Change Biology* 19.10, pp. 2932–2939.

R Core Team (2021). *R: A Language and Environment for Statistical Computing*. R Foundation for Statistical Computing. Vienna, Austria. URL: `https://www.R-project.org/`.

Redmond, Miranda D and Katharine C Kelsey (2018). "Topography and overstory mortality interact to control tree regeneration in spruce-fir forests of the southern Rocky Mountains". In: *Forest Ecology and Management* 427, pp. 106–113.

Scherrer, Daniel and Christian Körner (2011). "Topographically controlled thermal-habitat differentiation buffers alpine plant diversity against climate warming". In: *Journal of Biogeography* 38.2, pp. 406–416.

Smith, Taylor and Bodo Bookhagen (2021). "Climatic and biotic controls on topographic asymmetry at the global scale". In: *Journal of Geophysical Research: Earth Surface* 126.1, e2020JF005692.

Stage, Albert R (1976). "An expression for the effect of aspect, slope, and habitat type on tree growth". In: *Forest Science* 22.4, pp. 457–460.

Strobl, Katharina, Claudia Schmidt, and Johannes Kollmann (2018). "Selecting plant species and traits for phytometer experiments. The case of peatland restoration". In: *Ecological Indicators* 88, pp. 263–273.

Suggitt, Andrew J, Robert J Wilson, Nick JB Isaac, Colin M Beale, Alistair G Auffret, Tom August, Jonathan J Bennie, Humphrey QP Crick, Simon Duffield, Richard Fox, et al. (2018). "Extinction risk from climate change is reduced by microclimatic buffering". In: *Nature Climate Change* 8.8, pp. 713–717.

Theobald, David M, Dylan Harrison-Atlas, William B Monahan, and Christine M Albano (2015). "Ecologically-relevant maps of landforms and physiographic diversity for climate adaptation planning". In: *PloS One* 10.12, e0143619.

USGS (2019). *U.S. Geological Survey, 20190723, USGS 13 arc-second n43w113 1 x 1 degree*. `https://www.sciencebase.gov/catalog/item/5f7784fc82ce1d74e7d6cbec`.

Zellweger, Florian, Pieter De Frenne, Jonathan Lenoir, Pieter Vangansbeke, Kris Verheyen, Markus Bernhardt-Römermann, Lander Baeten, Radim Hédl, Imre Berki, Jörg Brunet, et al. (2020). "Forest microclimate dynamics drive plant responses to warming". In: *Science* 368.6492, pp. 772–775.

Supporting information

This supplemental document accompanies the paper, "A tree's view of the terrain: downscaling bioclimate variables to high resolution using a novel multi-level species distribution model," currently in review.

In addition to the supporting content included here, all R and Stan code and results are available on GitHub at [URL redacted for double-blind peer review]. The accompanying R package, which enables users to generate bioclimate estimates for any landscape across the study area, is available at [URL redacted for double-blind peer review].

APPENDIX 1: Supplementary methods

1.1 Topographic variables

We generated four topographic variables for every plot: northness, eastness, windward exposure, and elevational position. For a flat, level plot with an elevation that is average for its landscape, all four of these variables have a value of zero. We used a mix of topographic variables reported directly by FIA and NFI, and variables extracted from gridded digital elevation models at subplot locations using confidential exact plot coordinates. Both inventory datasets report slope and aspect recorded in the field for forest plots, which we used where possible.

In addition to the forest plots surveyed in the field, FIA also reports non-forest plot locations that were selected using the same gridded sampling scheme as the forest plots but were not visited for surveys because they were not forested. These locations provide valuable absence information for niche models (though nonforested plots may not be entirely devoid of trees since FIA's definition of forested is 10% canopy cover and no nonforest land use). We generated slope and aspect information for these plots since they do not have field-measured slope and aspect information. Using the coordinates for plot centers, we generated subplot coordinates based on the standard FIA plot geometry. For every subplot we then extracted slope, aspect, and existing vegetation type (EVT) from the LANDFIRE v. 2016 dataset, a 30 m resolution gridded dataset that is based on extensive field data and satellite imagery. EVT was used to exclude plot locations whose current land cover was classified as trees (since forests are already included in FIA surveys) or as water, agriculture, or developed (since species absences from these locations are not due to climatic suitability). This process added more than 470,000 locations in non-forested natural landscapes, for which we used slope, aspect, and geographic coordinates to derive additional topographic variables as described below. Non-forest plots were not added for Canada due to lack of available data, so the absence data for Canada comprise the set of forest plots where a given species did not occur.

Northness and eastness We converted slope (σ) and aspect (Θ) values into northness and eastness, where $northness = cos(\Theta)sin(\sigma)$ and $eastness = sin(\Theta)sin(\sigma)$. This refactoring avoids the use of a circular aspect variable (which would be incompatible with traditional regression analysis) and produces variables that are approximately linearly related with solar radiation (which on first principles makes them appealing microclimate regression predictors). Northness values range from -1 to 1 and represent how steeply a site is inclined toward the north, with larger negative values for steeper south slopes and larger positive values for steeper north slopes, while eastness does the same for the east-west axis; a plot with a southeast aspect would have positive eastness and negative northness. See figure S4 for a graphical illustration. Arbitrary aspect values are reported for plots with slopes less than 5% in FIA or less than 2% in NFI, so we set northness and eastness for these plots to zero to avoid bias. Plots that have been resurveyed multiple times occasionally have slight variation among surveys in measured slope and aspect; in such cases we calculated northness and eastness for each survey and then averaged them across surveys.

Windward exposure Windward exposure (ω) represents how a plot's windiness is expected to deviate from the average windiness of level sites on the local landscape. We extracted two wind variables describing local wind regimes—prevailing wind direction (D) and directional variability (V, the circular standard deviation of wind direction, weighted by wind speed)—from a gridded wind dataset at the locations of every plot.

Combining these with slope and aspect, we calculated windward exposure as $\omega = (1 - V)sin(\sigma)cos(\angle\Theta D)$, where $\angle\Theta D$ is the angle between Θ and D. ω approaches zero as wind direction becomes more variable (i.e. it does not blow in a consistent direction), as a plot becomes level, and/or as prevailing wind blows at a right angle to the plot aspect. It is increasingly positive as plots face more directly into the prevailing wind, and increasingly negative as plots face away from the prevailing wind. To make interpretation of ω consistent with northness and eastness, we rescaled ω values so that the difference in ω between due windward and leeward 30° slopes is 1 at the average value of V.

Elevational position Our final topographic variable was elevational position. This measures how a site's elevation compares to the elevation of the surrounding neighborhood, with positive values for hilltops and negative values for valley bottoms. While this variable is often called "topographic position index" (TPI), for clarity we avoid that term since all of our terrain variables represent topographic positions in a general sense. We calculated elevational position for each plot as the multiscale topographic position index ("mTPI" *sensu*); this is referred to as "multiscale" because it averages over a range of neighborhood sizes to incorporate topographic effects operating at multiple scales. We used neighborhood radii of 100 m, 225 m, and 500 m; the largest of these was chosen so it would not exceed the 1 km grid cells in the macroclimate data (thus ensuring that microclimate is informed by fine-scale topographic features not already reflected in the macroclimate data), while the others were chosen to create an evenly spaced log series. Elevational position calculations were based on (sub)plot coordinates and 30 m resolution gridded elevation data (LANDFIRE v. 2016 for the US, CDEM v. 1.1 for Canada).

1.2 Macroclimate variables

Using the coordinates of each plot, we extracted monthly temperature and precipitation data from CHELSA, representing climatic averages from 1979–2009 at a 1 km spatial resolution. This time period is expected to reflect climate conditions experienced during the majority of the lifetime of trees included in the analysis. From these monthly values we derived total annual precipitation, mean annual temperature, maximum temperature of the warmest month, and minimum temperature of the coldest month. These are variously treated as either "macroclimate variables" or "effect modifiers" (precipitation is used in both ways). For statistical normality and ecological relevance, we rescaled precipitation values by adding one and log-transforming them.

1.3 Data distillation

We excluded species occurring on fewer than 100 plots, and standardized all topographic and macroclimate values by subtracting the mean and dividing by the standard deviation. For each species, we then generated a distinct occurrence dataset representing presences and absences across climatic and topographic gradients. After cleaning, the final data set comprised 1,513,722 occurrences of 216 tree species across 504,422 (sub)plots, plus hundreds of thousands of absence records for each species. For each species we excluded absence records that were more than 10 degrees latitude or longitude beyond the bounding box encompassing plots where the species was present, in order to avoid absences arising from inaccessible rather than climatically unsuitable sites.

For computational reasons, it was necessary to reduce the number of observations in the data set before

fitting the Bayesian model. For each species we first excluded absences with macroclimate temperature or precipitation outside an expanded climatic bounding box (the range plus 20%) around the climate of plots where the species occurs, in order to avoid including absences with low information content about the species niche shape. Then we discretized the continuous data representing presences and absences across macroclimatic and topographic axes, converting it into a grid representing counts of presences and absences in discrete bins. Each of the seven predictors (three macroclimate and four topographic variables) was cut into four equal-interval bins spanning its range in the filtered data for a given species, and these bins were then intersected across the seven predictors to define a multidimensional grid, yielding a maximum of $4^7 = 16,384$ climate bins per species. (A sensitivity analysis (fig. S10) indicated that increasing the resolution to more than 4 bins per dimension had a negligible impact on inferred parameter values.) For each bin, the number of presences and absences of the focal species was recorded, reflecting both the proportion of presences and the total amount of available data. Means of the predictors (macroclimate, topographic, and modifier variables) were also calculated across plots for each bin, and were used in place of bin midpoints to increase precision in downstream analysis. Finally, the occurrence datasets for all species were combined into a single table, with an additional column identifying the species.

1.4 Statistical model

As noted elsewhere, our study uses three different variants of the statistical model described in this section. The "full multi-species" model jointly infers topoclimate effects from the distributions of all species in the dataset, and includes a layer that models how those effects vary across macroclimate gradients as a function of modifier variables; it is the primary subject of our empirical results. The "minimal single-species model" is a reduced version, which uses data on just one species and does not allow effects to vary with modifier variables. The "niche model" further simplifies the single-species model by eliminating the topoclimate effects and latent variable altogether and retaining only the species occurrence function described in equation 2; it is only used as part of the cross-validation analyses described below.

The bioclimate component of the full model represents how each of the four topographic variables modifies each of the three macroclimate variables to generate their corresponding latent bioclimate variables, with these effects varying according to the values of the two effect modifiers. It can be written as

$$\begin{aligned} m_{i,v} &= M_{i,v} + \sum_{t=1}^{4} (T_{i,t} \times B_{i,v} \cdot \delta_{v,t}) \\ \kappa &= d(\delta) \\ \delta &\sim N(0, 0.1) \\ \kappa &\sim exp(10^5) \end{aligned} \tag{1}$$

where i indexes the n rows in the dataset, v indexes the three climate variables, and t indexes the four topographic variables. m is a $n \times 3$ matrix of bioclimate, M is a $n \times 3$ matrix of macroclimate, T is a $n \times 4$ matrix of topographic variables, and B is a $n \times b$ matrix of spline basis functions of effect modifiers. δ is a $3 \times 4 \times b$ array of regression coefficients to be estimated, each with a weakly informative Gaussian prior.

The summation term represents the Δ anomalies introduced in the main text (figs. 1 & S1).

We used penalized tensor product splines to allow topographic effects to vary smoothly and nonparametrically across modifier values. The penalties prevent overfitting by limiting differences in the coefficients for adjacent basis functions; we used second-order differences to constrain the local curvature of the fitted surfaces. To generate B, we rank-transformed temperature and precipitation, generated a set of cubic spline bases for each transformed variable with eight evenly spaced knots, and then took all pairwise products between each of the temperature and precipitation bases, resulting in $b = 100$ basis products. κ is a vector of second-order differences between δ parameters for adjacent bases in each of the two dimensions, represented by the difference function d, penalized by restrictive priors.

The species niche component of the model represents species occurrence probabilities as a logistic regression function of the latent bioclimate variables m described above (or m can represent other predictors if the niche model is used as a standalone SDM), and a set of niche parameters:

$$
\begin{aligned}
y_{s,i} &\sim Binomial(n_i, p_{s,i}) \\
p_{s,i} &= \alpha_s e^{-.5(m_i-\mu_s)\Sigma_s^{-1}(m_i-\mu_s)^T} \\
\Sigma_s &= diag(\tau_s) L_s L_s^T diag(\tau_s) \\
\mu_s &\sim N(0,1) \\
\tau_s &\sim halfNormal(0,10) \\
L_s &\sim CholeskyLKJ(3) \\
\alpha_s &\sim Beta(1.5,3)
\end{aligned}
\tag{2}
$$

where y is the number of presences in a topoclimate bin, n is the number of plots in the bin, and p is the occurrence probability, with s and i indexing species and bins, respectively. Each species' niche is modeled as a three-dimensional Gaussian probability surface represented by the multivariate niche optimum μ and variance-covariance matrix Σ; this bell curve is scaled by the value α representing the species' occurrence probability at its niche optimum μ. Priors on these niche parameters are specified in the last four lines above. Plots of realized niche shapes (figs. 3 & S6) indicate that our assumption of bell-shaped niches is reasonable. Because species that occur on more plots are represented by higher occurrence counts and produce narrower binomial distributions, widespread species carry greater weight than rare species in influencing the posterior distributions of topoclimate parameters.

Model fitting jointly infers values of the topoclimate and niche parameters that best fit the observed species distribution data, given the assumptions of the model. While for simplicity our model assumes that suitability follows a multivariate Gaussian surface, this is not strictly necessary; the general latent-variable bioclimate modeling approach we introduce here would work with any SDM algorithm (including popular methods like random forest, Maxent, or Gaussian process) as long as it could be manually encoded in the multi-level model.

Bayesian modeling was done in Stan, via the *cmdstanr* R library. Using Stan's Hamiltonian Monte Carlo (HMC) algorithm, we ran five MCMC chains each with 500 warmup iterations and 1000 sampling iterations; note that HMC generally requires far fewer sampling iterations than traditional MCMC algorithms. MCMC behavior was evaluated by visual assessment of tracer plots and by diagnostic statistics including effective sample sizes, $\hat{r}$ values measuring convergence among chains, and the absence of divergent transitions.

1.5 Model evaluation

Diagnostics The MCMC ran with no divergent transitions. Model diagnostics indicate good mixing (via effective sample size, ESS) and convergence (via $\hat{r}$). For the δ parameters representing topoclimate effects, median $\hat{r}$ was 1.0010 (IQR: 1.0005–1.0017), median bulk ESS was 2722 (1833–4019), and median tail ESS was 3582 (2910–4030). For the species niche parameters, median $\hat{r}$ was 1.0005 (1.0001–1.0011), median bulk ESS was 4774 (3936–5396), and median tail ESS was 3798 (3225–4462). ESS was calculated across samples from all chains; note that ESS can be larger than the number of posterior samples in HMC. Model outputs including diagnostic summaries and posterior draws for all 9,165 model parameters are included in the project repository.

Simulations We used simulated data to test the model's ability to correctly infer topoclimate parameters. To make the simulated dataset realistic, including non-idealized data features like covariance among predictors, we began with the empirical dataset used in our main analysis and simply replaced the dependent variable (species presence/absence) with a simulated version of itself. We generated randomly sampled "true" topoclimate effect parameters (δ_{true}), combined them with the predictor data (macroclimatic, topographic, and modifier variables) to calculate microclimate, and then combined microclimate with randomly generated niche parameters to simulate species occurrences. We then fit the model on the simulated dataset using maximum likelihood estimation to find the posterior mode, and compared the inferred δ parameters to their true values. The statistical model performed well in recovering the known parameters ($r^2 > 0.999$; $RMSE/sd(\delta_{true}) = 0.055$); fig. S12–S13). This confirms the ability of our statistical machinery to correctly infer topoclimate effects given the assumptions of the generative model.

Macroecological predictions Another approach to assessing model fit is to test its ability to reproduce the emergent biogeographic patterns shown in figure 3. We used the model input data and the fitted model to predict each plot's fine-scale bioclimate from its macroclimate and topography, and then to predict species occurrence probability from bioclimate. We then used the fitted niche model parameters for each species to center and scale macroclimate values relative to each species' climate niche, representing a plot's microclimate as a location within the species niche, and then summarized across species to produce predictions analogous to figure 3d. Comparing these predictions to the observed data, we find that the model reproduces these empirical patterns quite well (with somewhat smaller topographic differentiation than in the observed data, as expected given conservative priors) (fig. S11).

Comparison to macroclimate in predicting occurrences To be valuable, our inferred bioclimate estimates would need to be more useful than standard macroclimate variables in predicting ecological patterns. Though the goal of BISOHP bioclimate variables is not primarily for use as predictors in SDMs, their performance relative to macroclimate variables in predicting tree species distributions serves as an accessible test of their ecological relevance.

We conducted this comparison for both the full multi-species model across the entire dataset and the minimal single-species model fit separately on each of the 216 species. In both cases we evaluated model predictions using both "within-sample performance" (closely related to ΔAIC) and "out-of-sample performance" (i.e. cross-validation). For each of the four analyses, we summarized the point-wise performance metrics in four different ways, for a total of 16 final performance indicators; while it adds some complexity, we report results for this array of methods rather than just a single method in order to assess sensitivity to arbitrary modeling choices.

The details varied among these four analyses as outlined below, but each involved fitting a bioclimate model, using it to estimate bioclimate across a set of FIA plots, and then using log likelihood to compare the performance of these bioclimate variables versus standard macroclimate variables as predictors of species occurrences in a niche model. "Niche model" here refers to use of the niche submodel described in equation 2 as a standalone model rather than coupled to the topoclimate model. We performed these validations using penalized maximum likelihood (ML) fits identifying the posterior mode, rather than full Bayesian posteriors, because the latter would have been too computationally intensive for use with cross-validation.

The following routines describe our process for computing the four performance metrics for each species:

1. **Within-sample performance, full multi-species model:**
   (a) Fit a BISHOP model on the full data set
   (b) Use the fitted parameter values to calculate inferred bioclimate variables for each data point
   (c) For each species:
      i. Fit one niche model as a function of the bioclimate variables, and another as a function of the macroclimate variables
      ii. Use these models to predict the occurrence probability for each record in the data set, and compute the log likelihood of the observed presence/absence data given these predictions
      iii. Calculate delta log likelihood, ΔLL, for each data point as the difference between the log likelihoods of the bioclimate- and macroclimate-based models; this value is positive when the bioclimate variables yield better predictions for a given data point, and negative when the macroclimate variables perform better
2. **Within-sample performance, minimal single-species model:**
   (a) For each species:
      i. Fit a BISHOP model on the data set for that species
      ii. Use the fitted parameter values to calculate inferred bioclimate variables for each record for that species
      iii. Proceeded as with steps *1.c.i–iii* above.
3. **Out-of-sample performance, full multi-species model:**
   (a) Randomly assign each species to one of ten data partitions
   (b) For each partition, fit a BISHOP model using the data for the species in the other partitions, and use it to predict the bioclimate for data points in the focal partition
   (c) For each species:
      i. Randomly assign each data point to one of ten partitions
      ii. For each partition:

A. Using predictor data for the other ("training") partitions, fit one niche model as a function of the bioclimate variables, and another as a function of the macroclimate variables
B. Use these models to predict the occurrence probability for each record in the focal "testing" partition
C. Compute ΔLL as in step *1.c.iii* above

4. **Out-of-sample performance, minimal single-species model:**
   (a) For each species:
      i. Randomly assign each data point to one of ten partitions
      ii. For each partition:
         A. Using predictor data for the other ("training") partitions, fit a BISHOP model using data from the other partitions, and use it to predict the bioclimate for those same training data
         B. Proceed as with steps *3.c.ii.A–C* above

These procedures gave within-sample an out-of-sample ΔLL values for the minimal and full models for each record in the data set. For each of these four metrics, we next calculated the sum and the mean of the point-wise ΔLL values for each species. The sum reflects the total amount of performance evidence across a data set and is the metric typically used in model selection, while the mean reflects expected performance independent of data set size. For within-sample predictions, the sum is closely related to ΔAIC (we did not compute ΔAIC itself due to the challenge of computing the number of effective parameters in a hierarchical model).

To draw conclusions about whether bioclimate outperformed macroclimate in general across species, for each metric we used a non-parametric Wilcoxon's signed-rank test on the 216 species-level sums or means. For each Wilcoxon's test we computed one version with species weighted equally (reflecting performance for the typical tree species), and a second version with species weighted by the number of occurrences in the data set (reflecting performance for the typical tree).

The results of these analyses are reported in figure S14.

Comparison to standard SDM with macroclimate and topographic predictors The above analyses demonstrated that bioclimate does outperform macroclimate as a predictor of species distributions (fig. S14). This indicates that the bioclimate variables are useful for ecological studies seeking downscaled climate data or seeking insight into topography-bioclimate relationships, which are the primary purpose of BISHOP. But for studies that do not seek insight into fine-scale climate patterns for their own sake but rather aim simply to predict species distributions, it leaves open the question of whether the unique latent variable structure of BISHOP is any better than a more standard SDM that includes both topography and macroclimate as predictors.

To assess this, we compared minimal single-species BISHOP models for every species to a model that included the same set of topography and macroclimate variables as separate predictors. (The full multi-species model was not used for this comparison, since without the bioclimate term it is equivalent to separate minimal models.) Many alternative model formulations would be possible for the comparison model, but we chose a version that was a similar as possible to BISHOP, with the three macroclimate variables influencing

occurrence probability as a multivariate bell-shaped surface, and the four topographic variables each having logit-linear effects on occurrence probability. Ten-fold cross-validation was used as above, with predictive performance quantified on withheld testing data using point-wise log predictive likelihood and also using area under the receiver-operator curve ("AUC"). Wilcoxon's tests were used as above to test the significance of the distribution of performance differences across species.

The results of these evaluations are reported in figure S15. We found that the models have similar predictive accuracy, with BISHOP performing either better or equivalently depending on the performance metric. This suggests that the BISHOP model structure is useful as an SDM, even though its primary purpose is to model bioclimate, not to model species distributions. However, if simply predicting occurrences is the primary goal of a study, then a traditional SDM with macroclimatic and topographic variables may be just as good as the more complex BISHOP approach.

APPENDIX 2: Supplementary figures

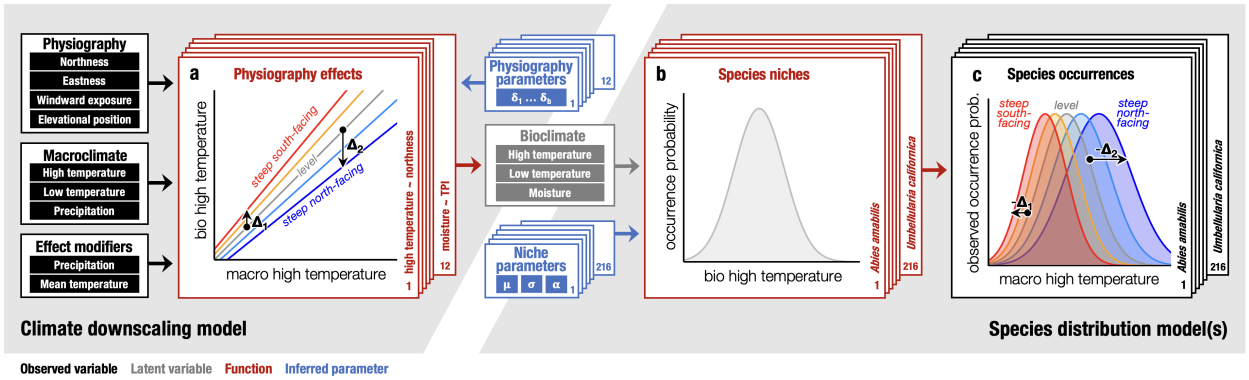

Supplemental figure S1: Illustration of the multi-level BISHOP model used in our emprical analysis. It is assumed that the combination of macroclimate and physiographic variables like topography or vegetation jointly shape fine-scale bioclimate via a set of physiography effects **(*a*)**, and that bioclimate in turn shapes species distributions via their climatic niches **(*b*)**, with these processes together manifesting as observed differences in species occurrences across gradients of macroclimate and fine-scale physiography **(*c*)**. A site's bioclimate is treated as an unmeasured latent variable, and modeled as macroclimate plus a deviation, Δ, which is a function of physiography and assumed to be zero on level ground; the non-parallel lines in panel *a* illustrate that the sizes of physiography effects can themselves vary as a function of "effect modifying" variables. Species niches are modeled as functions of bioclimate, rather than macroclimate as in a typical SDM. For a given shift in local physiographic position, the change in the macroclimate that a species occupies while holding its occurrence probability constant (horizontal shifts in panel *c*) corresponds to the change in bioclimate while holding macroclimate constant (vertical shifts in panel *a*, e.g. Δ_1 and Δ_2). As a result, the topoclimate effects illustrated in panel *a* can be inferred from the biogeographic patterns in panel *c*, by jointly inferring all parameters in the multi-level statistical model. Note that for simplicity, the graphs in panels *a*–*c* depict one species, one climate variable (high temperature), and one physiographic variable (northness) with discrete levels; our full empirical analysis jointly infers parameters for 216 species, three climate variables, and four continuous topographic variables.

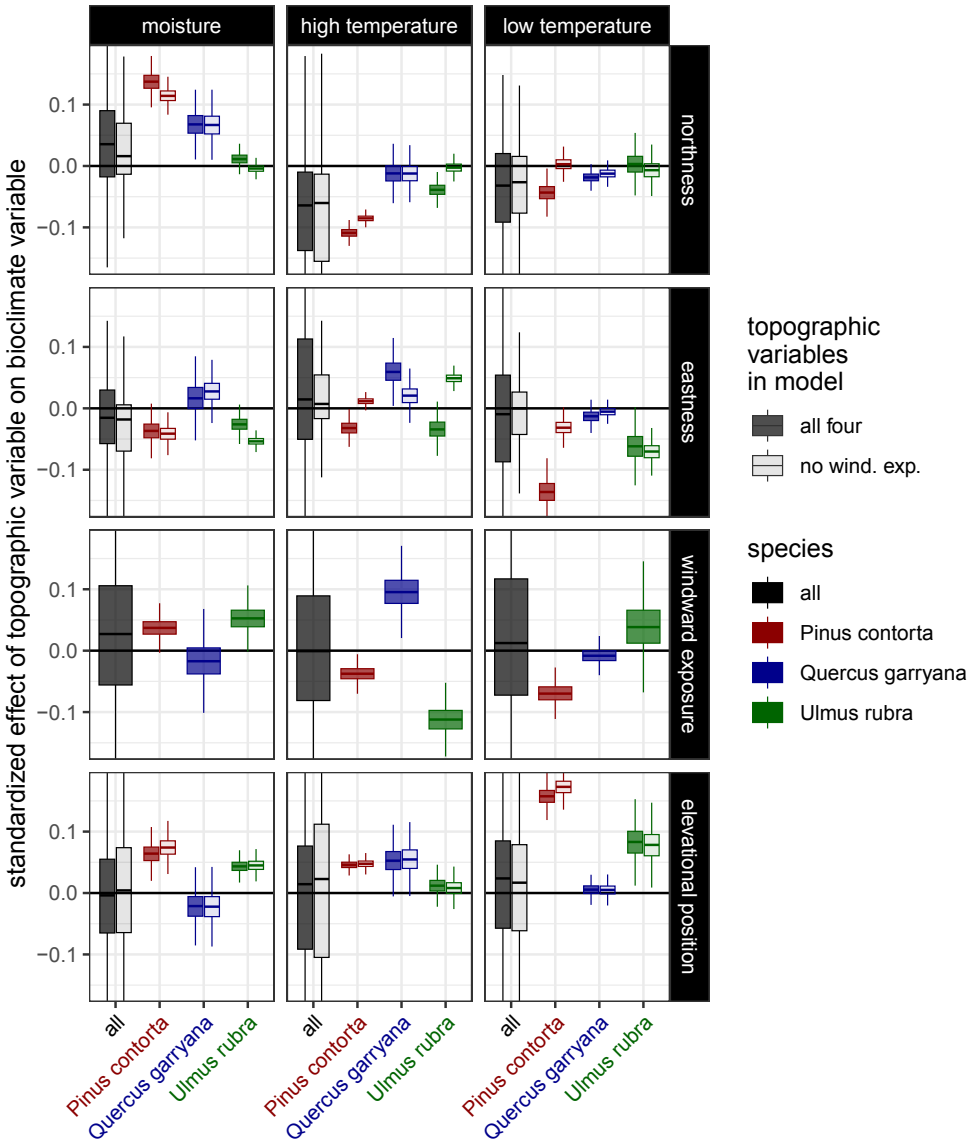

Supplemental figure S2: Inferred topoclimate effects from the minimal single-species models. Y-axis values are the standardized effect slopes of the linear relationship between the topographic variable listed at top and the bioclimate variable listed at right. Each colored boxplot is the distribution over posterior samples from a single model for one example species, while each black boxplot is the distribution over posterior modes from 216 separate models for each species. Opaque boxes are the results for the model with all four topographic variables, while transparent boxes are from the model with only northness, eastness, and elevational position. (See also figs. 4 and S5, which show analogous results for the full multi-species model.)

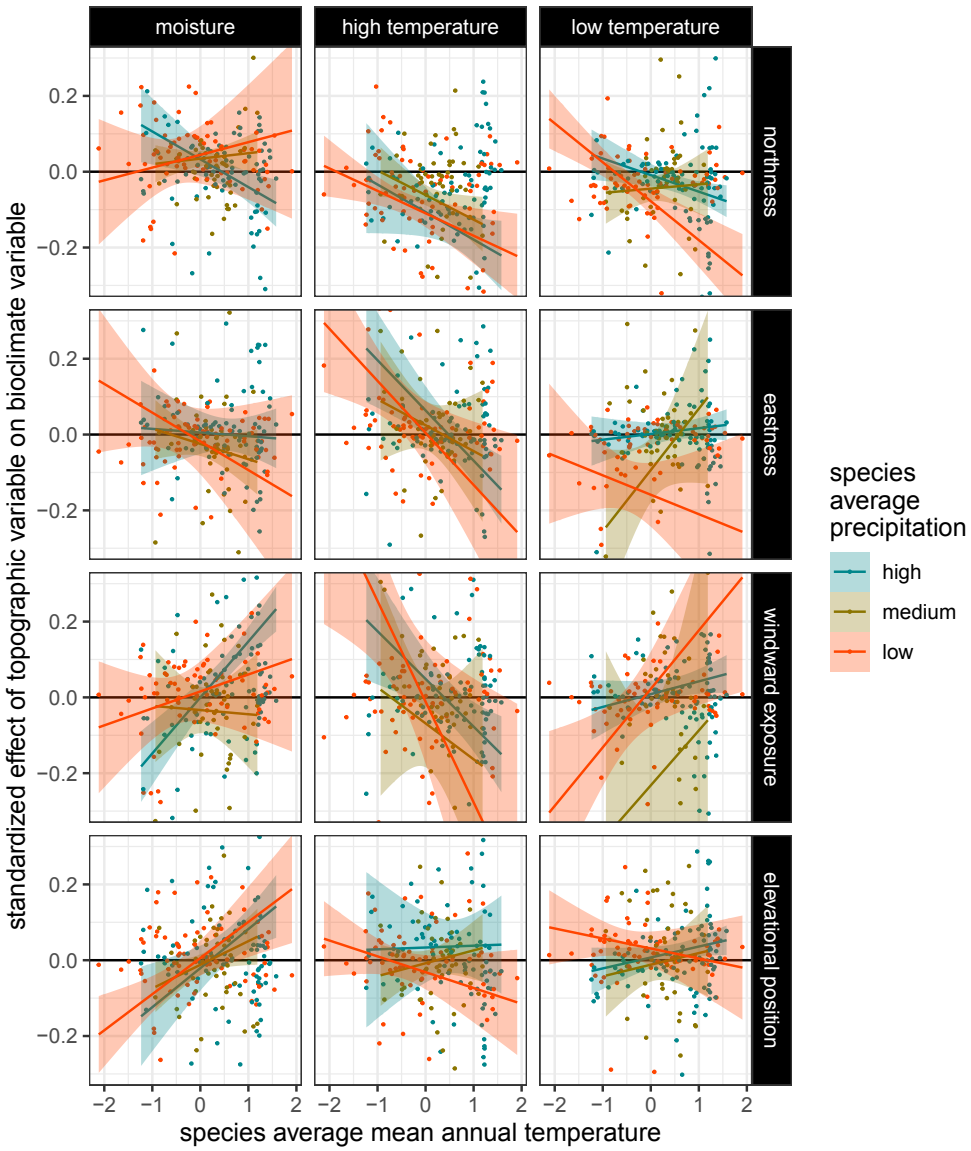

Supplemental figure S3: Relationships between topoclimate effects from each of the 216 minimal single-species models, and the mean temperature and precipitation across each species' range. X-axis values are standardized mean annual temperature, colors are precipitation terciles (i.e. species from dry, medium, and wet regions), and y-axis values are standardized effect slopes of the linear relationship between the topographic variable listed at top and the bioclimate variable listed at right. Lines and shaded regions are linear models with 95% confidence intervals.

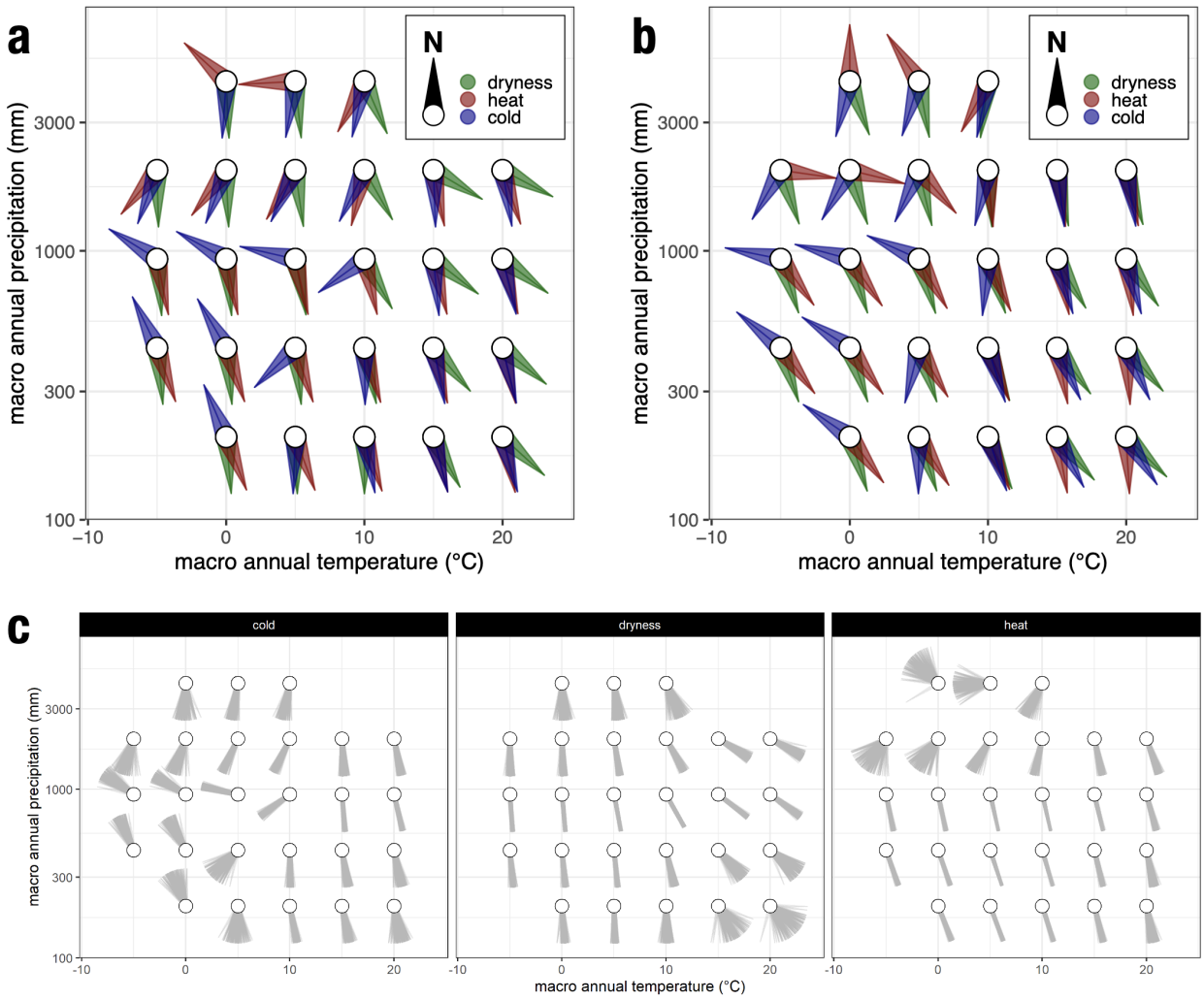

Supplemental figure S4: Aspects of maximum bioclimate differentiation, calculated from northness and eastness effects. The grid of points represents effects for different points in macroclimate space and corresponds to the grid in figure 4a. The arrows show the compass direction of the local hillslopes on which a given bioclimate variable is maximized according to the fitted model (they indicate a direction in *geographic* space, not a direction on the x-y climate grid). For moisture, negative effects ("dryness") are shown so that they better align with temperature effects for comparison. **(a)** Posterior medians for the model *excluding* windward exposure, which can be interpreted as the overall aspect of bioclimate differentiation. **(b)** Posterior medians for the model *including* windward exposure, which could be interpreted as the aspect of sun-based bioclimate differentiation since wind is controlled for separately from the northness and eastness effects shown here. **(c)** Samples from the posterior distribution for the model excluding windward exposure, representing uncertainty around the medians shown in *a*; 100 random samples are shown.

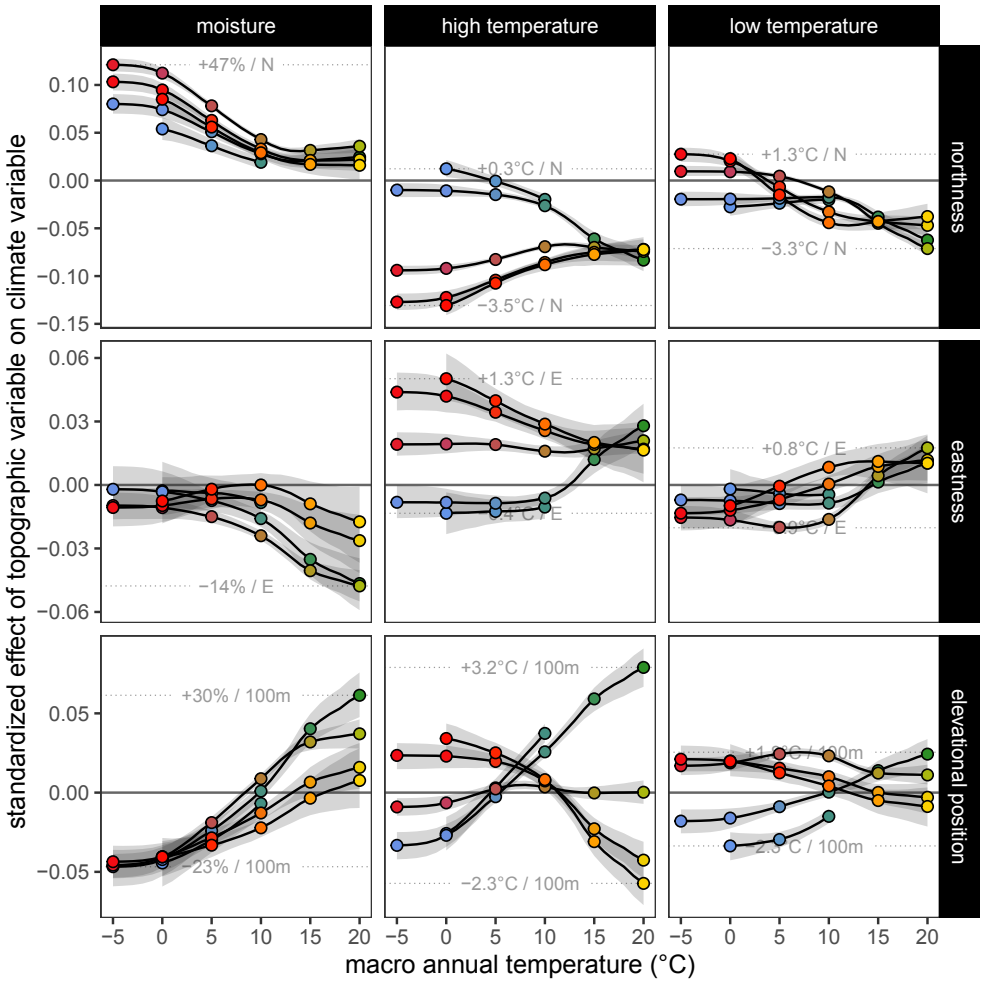

Supplemental figure S5: Topoclimate effects for the model without windward exposure. See figure 4 for description and comparison.

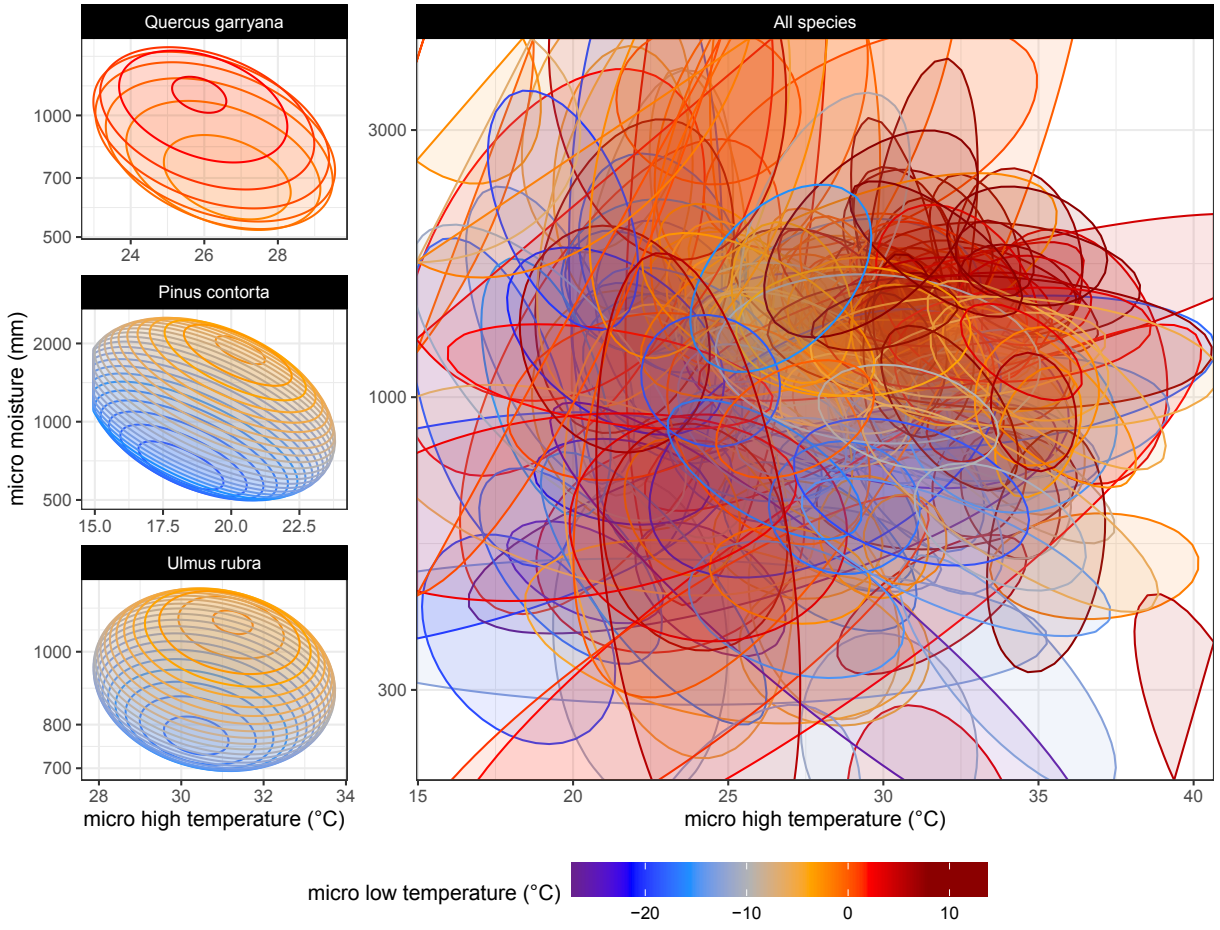

Supplemental figure S6: Inferred bioclimatic niches for three example species **(a-c)** and for all 216 species in the analysis **(d)**. For each species, this illustration shows one probability contour of the full three-dimensional niche surface, at 50% of the species' maximum occurrence probability; because the niches are multivariate Gaussian surfaces, the 50% contours are ellipses in two dimensions (d) and ellipsoids in three dimensions (a-c), with probability gradients (not pictured) decreasing outside the contour and increasing to 100% of the species maximum at the center of the contour. The x- and y-axes show high temperature and moisture, while the third niche dimension, low temperature, is represented in color. In a-c, all levels of low temperature that contain the 50% contour are shown, illustrating the full three-dimensional ellipsoid; in d, only the largest contour, at the level that slices through the center of the ellipsoid and contains the climate optimum, is shown. All illustrations here show the posterior mode.

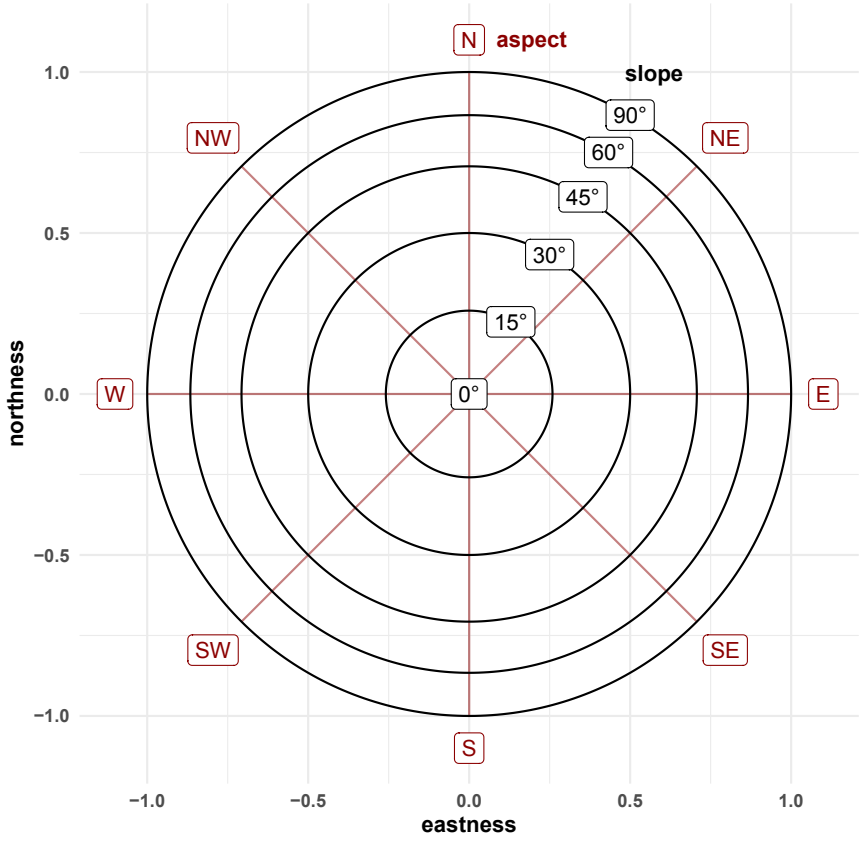

Supplemental figure S7: Geometric relationship between the polar slope-aspect coordinate system and the Cartesian eastness-northness coordinate system, where $northness = cos(aspect)sin(slope)$ and $eastness = sin(aspect)sin(slope)$, with slope and aspect measured in radians. For example, a northwest-facing 45-degree slope, a north-facing 30-degree slope, and a northeast-facing 45-degree slope all have northness values of 0.5, while they have eastness values of -0.5, 0, and 0.5, respectively.

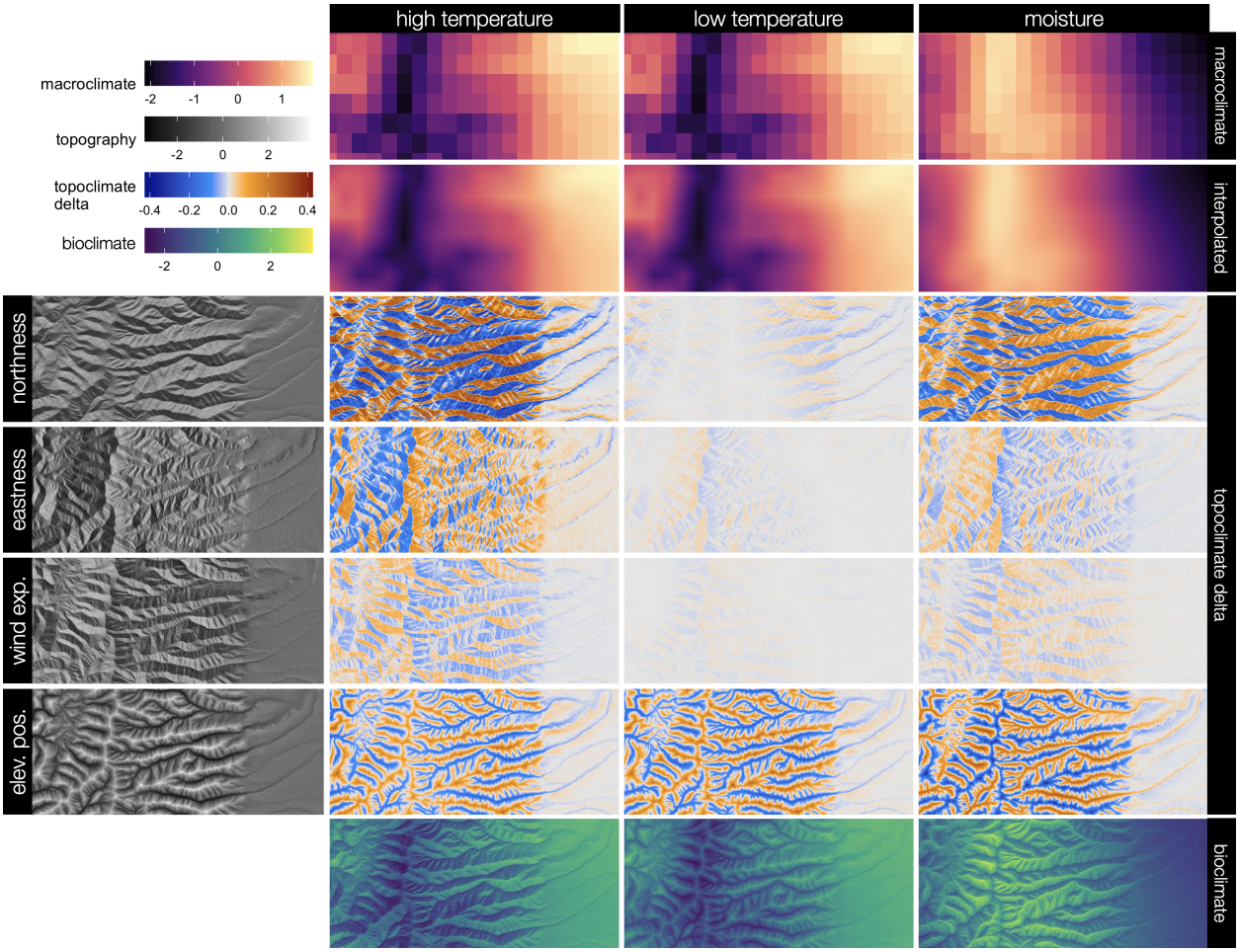

Supplemental figure S8: Data inputs and intermediate steps for the climate downscaling process shown in figure 5. The procedure begins with 10 m elevation data and wind data (not pictured), which are converted into the four topographic variables shown in the leftmost column. 1 km macroclimate data (top row) are interpolated to 10 m (second row). For each combination of climate variable and topographic variable, topoclimate deltas (central panels) are calculated based on topography, interpolated macroclimate, and the topoclimate model parameters inferred from tree species distributions; these deltas represent the local deviations from macroclimate resulting from a given topographic variable. Lastly, bluebioclimate (bottom row) is calculated by summing macroclimate and the four deltas. For visualization purposes this figure shows standardized values for all variables.

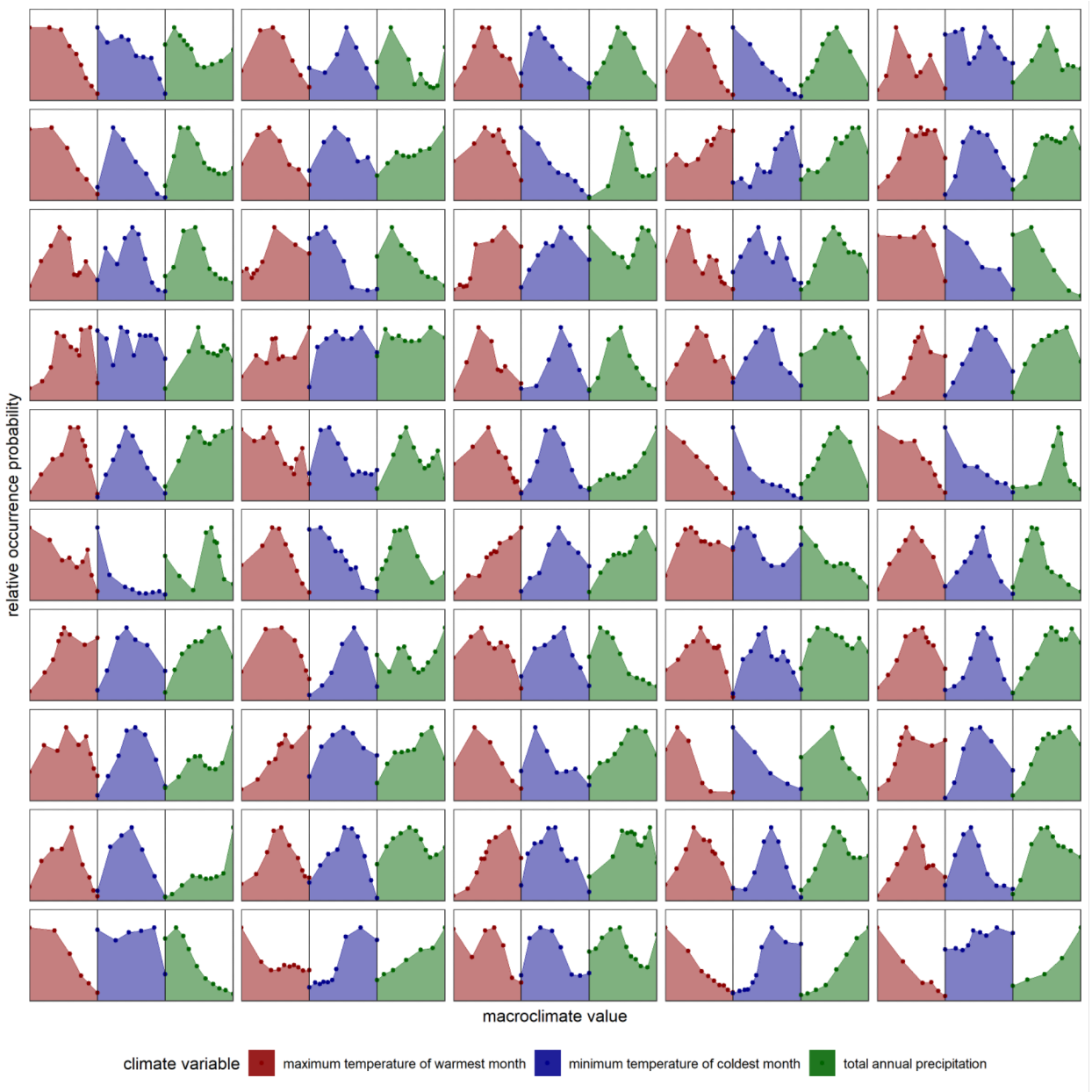

Supplemental figure S9: An evaluation of the assumption that species niche shapes are Gaussian. This figure shows realized niche data for three macroclimate variables for 50 random FIA species. For each variable, the x-axis spans the range of climates where the species is found, with points at each decile of species occurrence. The y-axis shows the fraction of plots in a given decile bin where the species occurred, considering only plots within the rectangular latitude-longitude bounding box encompassing presences for that species. Most of these species exhibit the general features of a bell curve—a unimodal occurrence pattern that declines asymptotically at similar rates on both sides of the peak—suggesting that the Gaussian niche form we use in this study is a reasonable choice. Note that the peak of the bell curve need not be contained within the observed data range for a Gaussian function to fit the data well (e.g. the species in the lower right corner exhibits monotonic relationships with all three climate variables across the range of observed climates, but these relationships can still be fit well with a Gaussian curve).

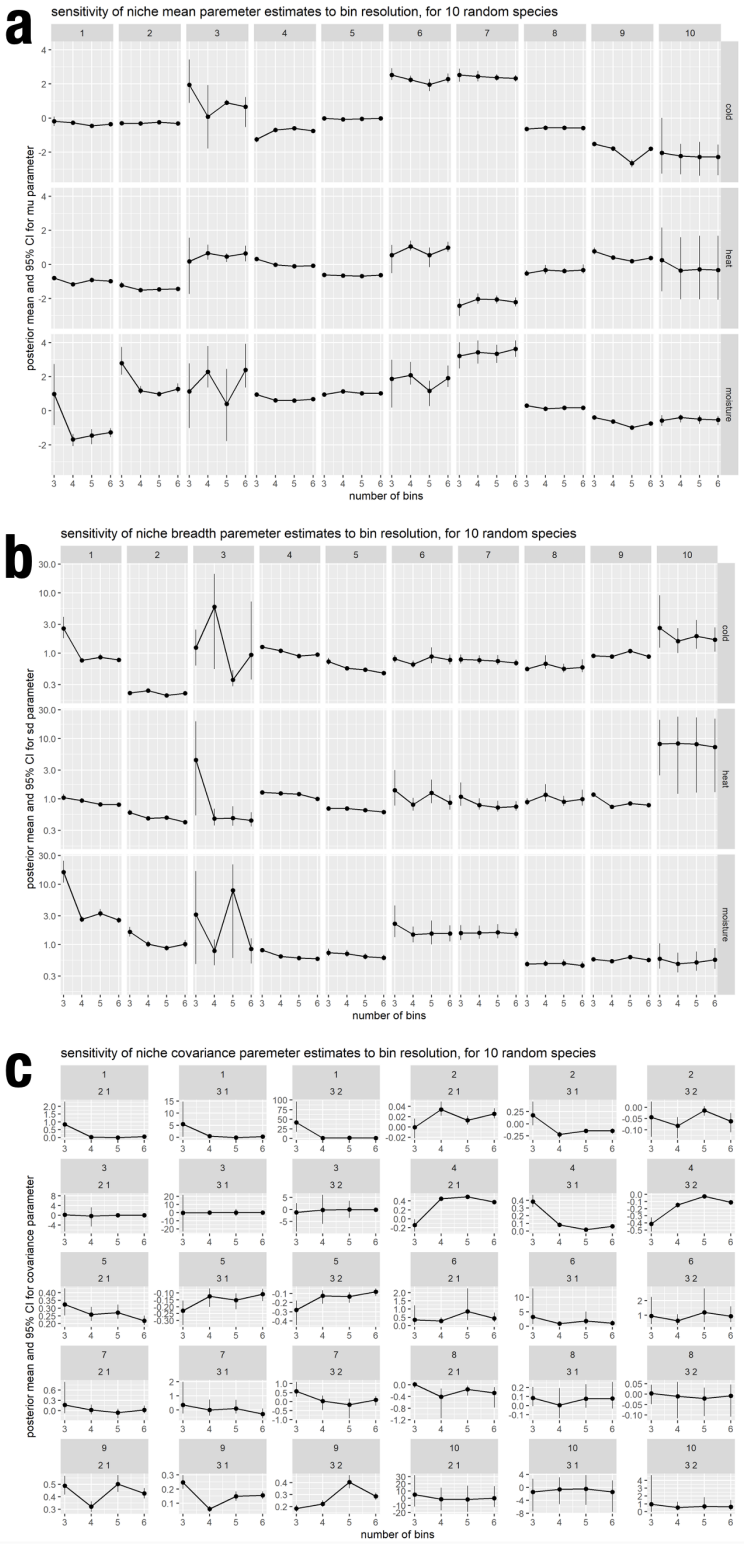

Supplemental figure S10: Sensitivity analysis of the effect of bin resolution on inferred species niche parameters. Due to computational time, this analysis was done with ten random species, denoted by the integers 1-10. Niches are parameterized as multivariate Gaussian surfaces defined by **(a)** means, **(b)** variances, and **(c)** covariances. Points and whiskers represent posterior means and 95% credibility intervals. Panel *c* has a subplot for each species for each pair of climate variables. Overall, parameter estimates using 4 bins per dimension were very similar to estimates using a larger number of higher-resolution bins, indicating that increasing the grid resolution does not substantially affect model results. Four bins per dimension were used in the main analysis due to the exponential relationship between bin number and computational burden.

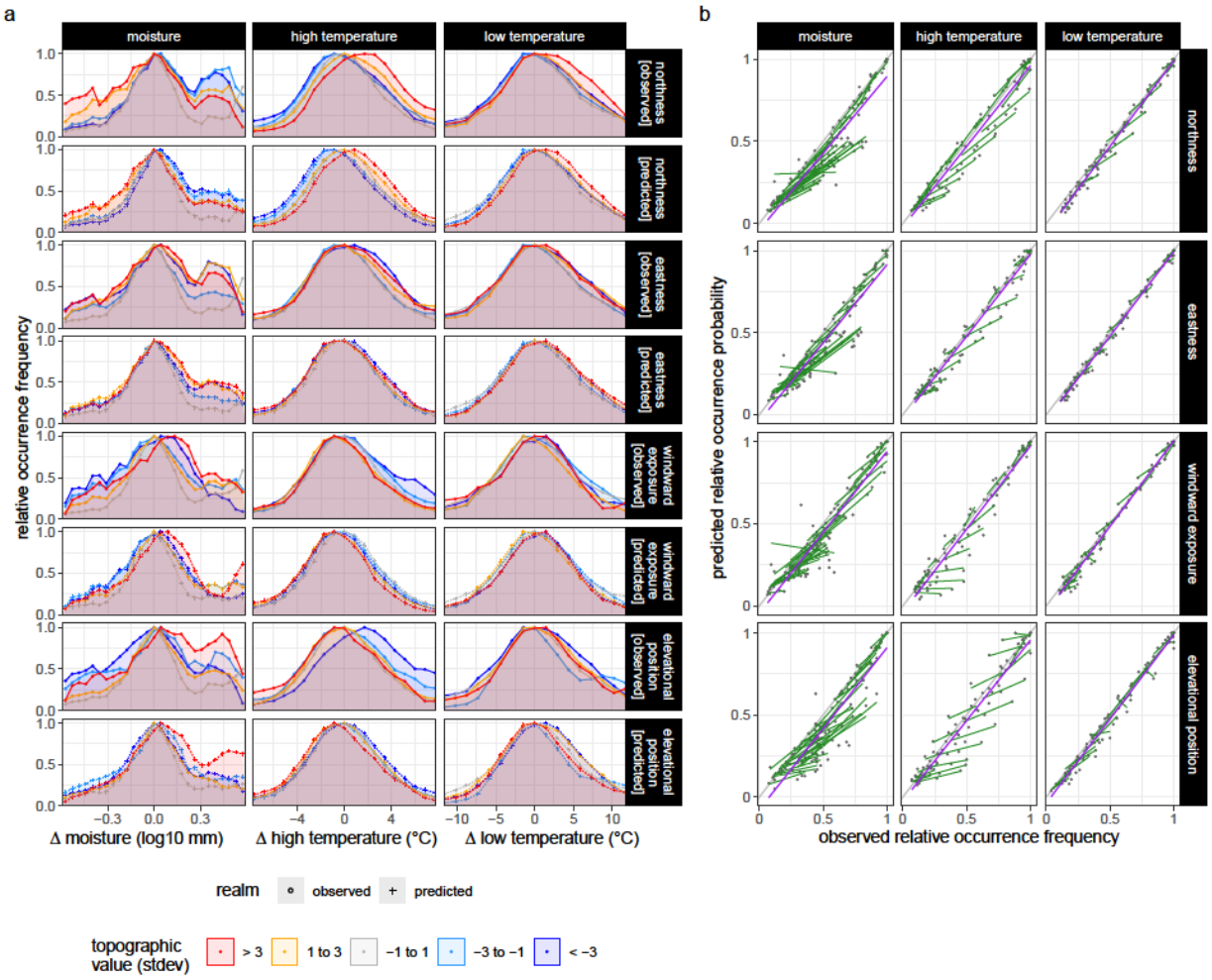

Supplemental figure S11: Observed versus predicted topographic species occurrence patterns for the average tree species, comparing the empirical patterns shown in figure 3 to predictions from the fitted model. **(a)** Observed and predicted species occurrence curves for each of the 12 topography-climate relationships; the observed data are repeated exactly from figure 3d of the main text (see that figure's caption for details), with the corresponding model predictions shown in the panel immediately below each observed pattern. **(b)** Observed versus predicted probabilities for each relationship, with a point for each of the points in panel *a*. The purple lines show linear fits across the full set of points for each relationship. The green lines show linear fits across the five points that share a given x-axis value in panel *a*; these are closely related to topoclimate effects, are positively sloped when the model correctly identifies the direction of the topoclimate effect, and have slopes of 1 when the model perfectly matches the observed data (which is not necessarily a goal as it could indicate over-fitting).

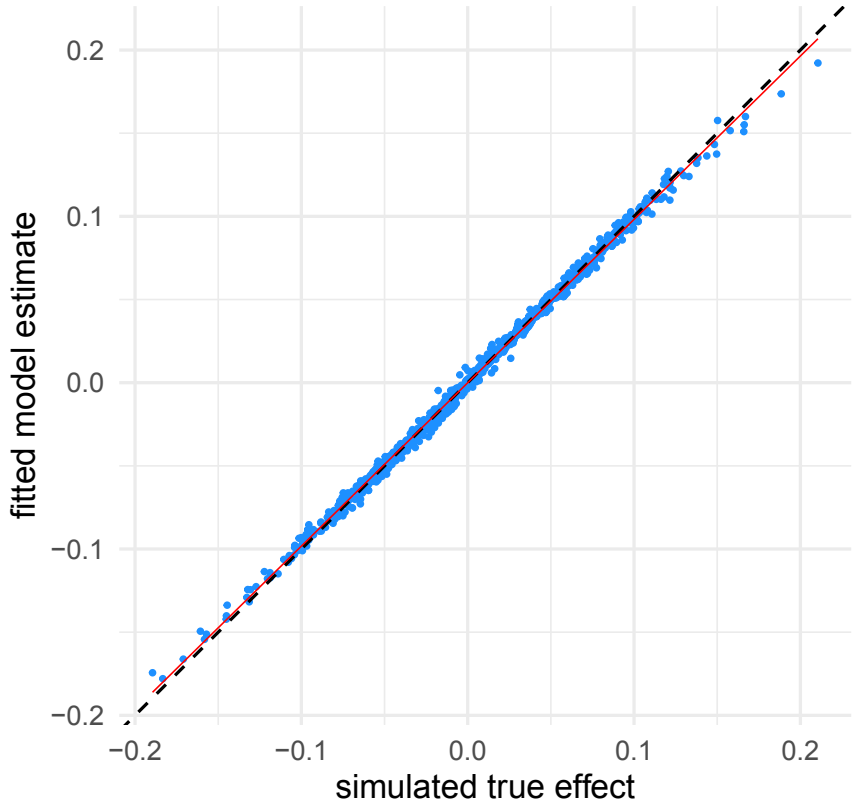

Supplemental figure S12: Model performance on simulated data. Each point corresponds to a δ parameter, with one δ for each topographic variable, for each climate variable, for each basis function of the modifier variables. The x-axis shows the known coefficient (sampled from a normal distribution) used to simulate the data, while the y-axis shows a penalized maximum likelihood estimate (posterior mode) of the coefficient. The dashed black line is the 1:1 line while the solid red line is a linear fit across points. R-squared = 0.999. See figure S13 for additional detail.

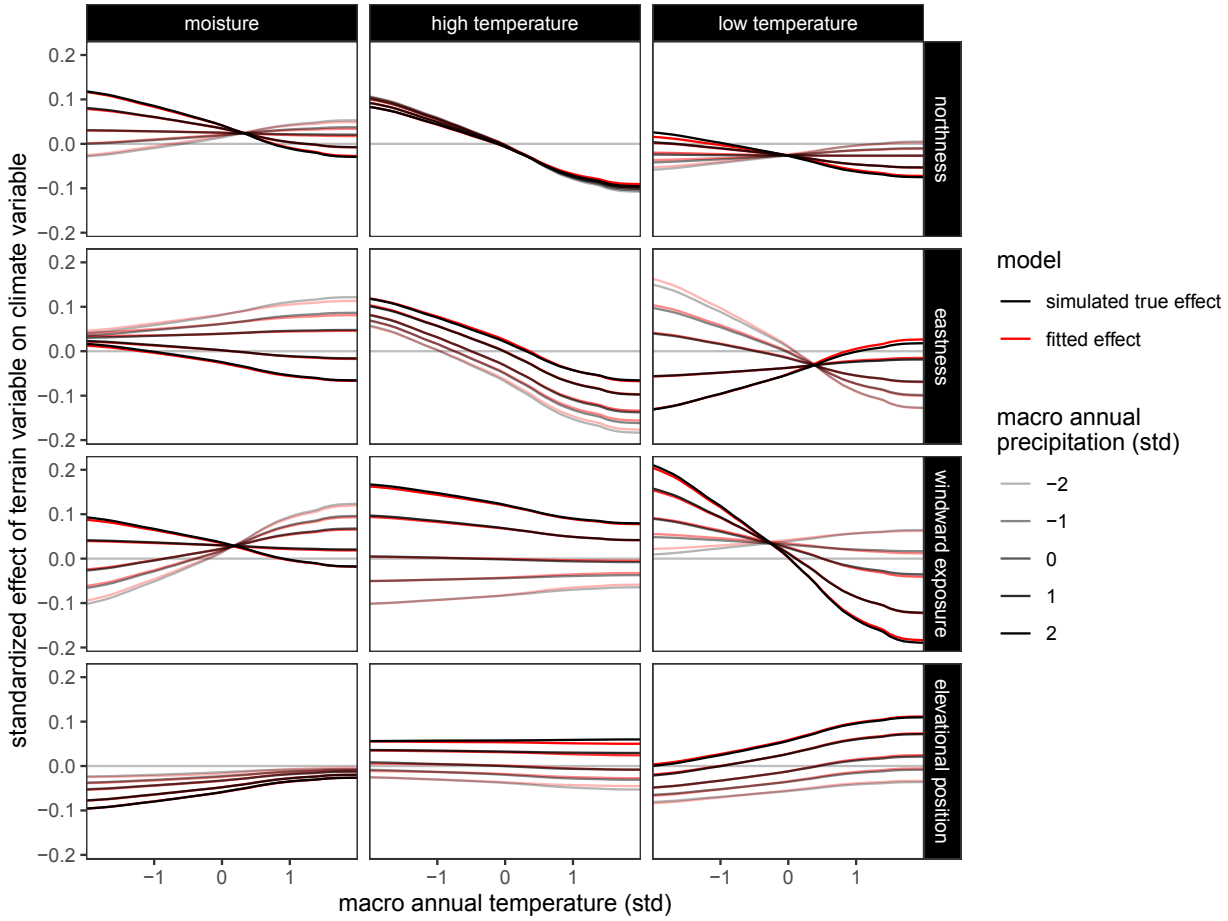

Supplemental figure S13: Model performance on simulated data, further illustrating the parameters shown in figure S12. In this figure, those parameter values were used to generate splines representing how topoclimate effects (y-axis) vary as a function of modifier variables (x-axis and line transparency). The black curves show the "true" randomly generated topoclimate effects used to simulate the test data, while the red curves show the fitted values estimated from the simulated data.

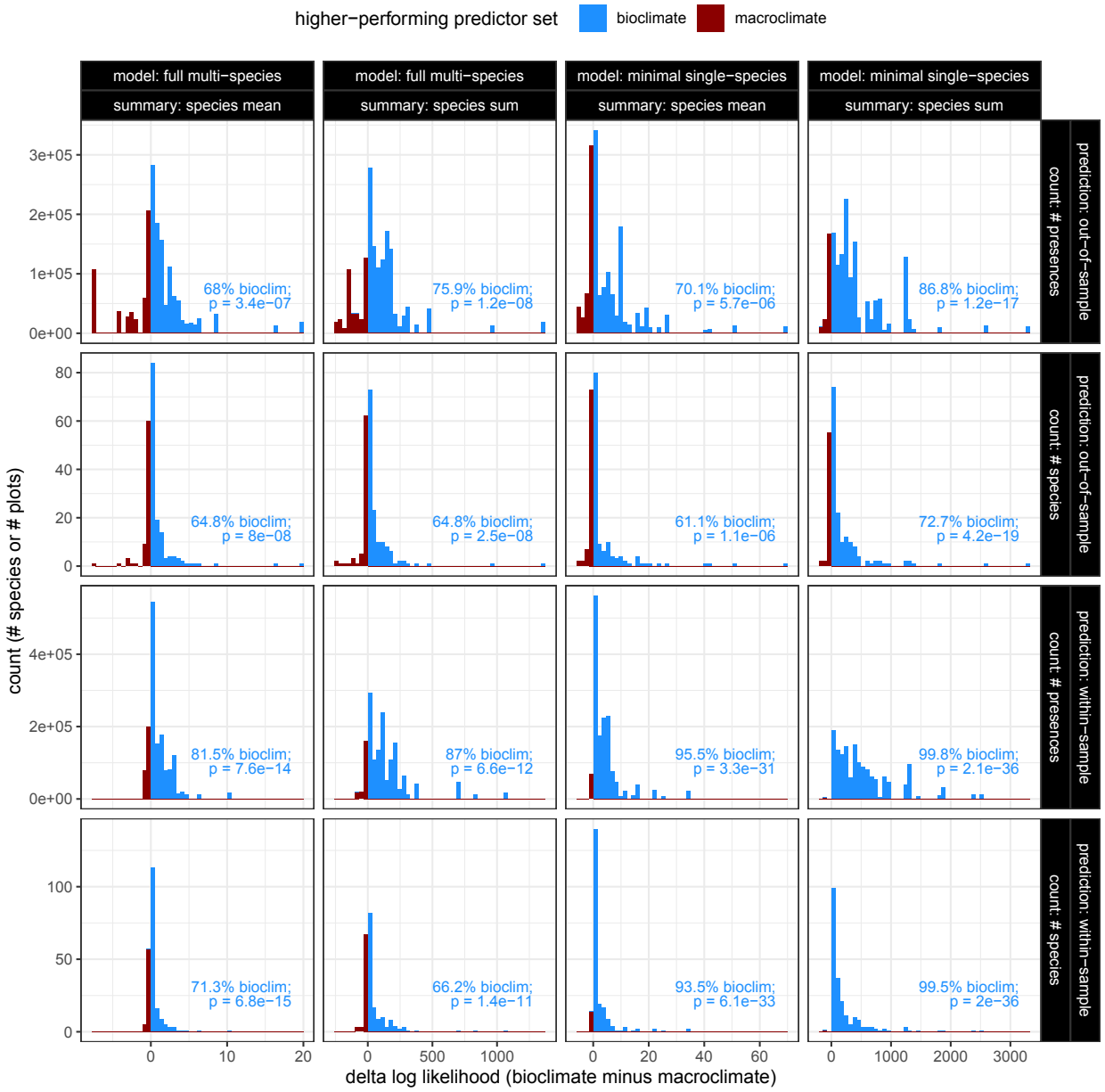

Supplemental figure S14: Results of model validation analyses comparing predictive performance of inferred bioclimate variables versus macroclimate variables. The histograms show distributions across species of delta log likelihood values, with positive (blue) values indicating that bioclimate variables outperform macroclimate variables in predicting species distributions, and negative (red) values indicating the opposite. The text annotations indicate the proportion of species or plots for which bioclimate variables outperformed macroclimate variables, and the statistical significance of the bioclimate-macroclimate difference according to a paired Wilcoxon signed-rank test. Each facet of the figure shows results from a different variant of the validation analysis, as indicated by the labels at the top and right edges. Differences between the "full" versus "minimal" model, and between the "within-sample" versus "out-of-sample" predictions, are described in appendix 1.5. The other variations refer to how the likelihoods were summarized across the dataset: "species sum" versus "species mean" indicates whether likelihoods were summed per species (as typical in AIC, e.g.) or averaged (an indicator that is more independent of dataset size), while "# species" versus "# presences" indicates whether the histograms and annotations reflect one point per species or are weighted by species abundance in the data set (arguably more relevant in understanding forests generally).

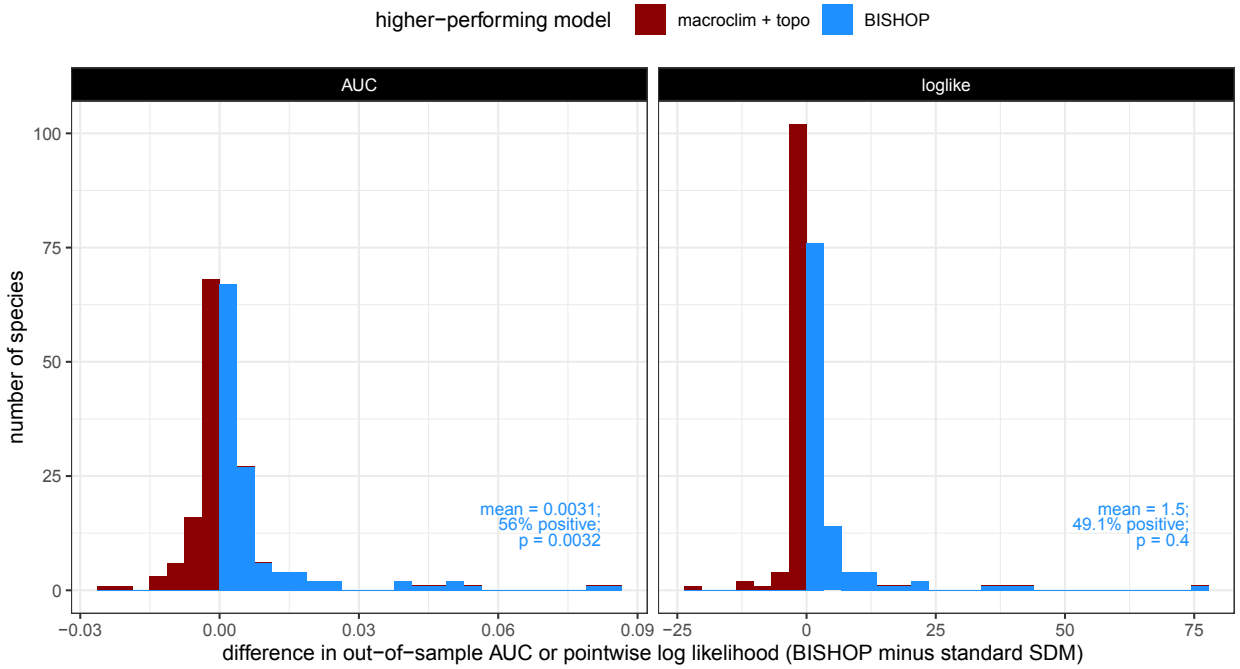

Supplemental figure S15: Evaluation of accuracy in predicting out-of-sample occurrences during cross validation, comparing BISHOP to a standard SDM fit with the same seven topographic and macroclimatic predictors but without the bioclimate interaction term. The histograms show distributions across species of performance differences in either area under the receiver-operator curve ("AUC") or point-wise log likelihood ("loglike"), with positive (blue) values indicating that BISHOP performed better in predicting species distributions, and negative (red) values indicating the opposite. The text annotations indicate the mean difference, proportion of species or plots for which BISHOP performed better, and statistical significance of the difference according to a paired Wilcoxon signed-rank test.